SEISMOLOGICAL INVESTIGATIONS AT THE GEYSERS GEOTHERMAL FIELD

E. L. Majer

T. V. McEvilly

Seismographic Station
Department of Geology and Geophysics
and
Lawrence Berkeley Laboratory
University of California
Berkeley, California 94720

December, 1977

This work was done with support from the
U.S. Department of Energy

CONTENTS

ABSTRACT

Two short (4 and 6 days) recording periods at The Geysers geothermal field provided useful data on two large refraction explosions and numerous microearthquakes. The vapor-dominated reservoir appears to be characterized by regionally anomalous high P- and S-wave velocities and low attenuation, but the anomaly seems to decrease, possibly reversing, with depth. Microearthquakes occur in a diffuse pattern, with no indication of dominant throughgoing faults and an absence of activity in the main production zone. Mechanisms are generally consistent with NE-SW compression. Occurrence rates indicate a slightly high incidence of smaller magnitude shocks. It is possible that the microearthquake activity is related to an expanding steam zone. While the present anomalies appear to delineate the reservoir, it is not certain that they would have been detectable in an exploration mode, prior to large-scale exploitation of the field.

I. INTRODUCTION

In an investigation of the utility of seismological observations for geothermal reservoir evaluation, a 13-station linear array of short-period vertical seismographs was set out across The Geysers geothermal field in northern California. The study was prompted by the planned detonations of two one-ton explosive sources, 8 and 18 km west of the field (See Figure 1), for an unrelated U.S. Geological Survey (USGS) refraction study. In addition to the two explosions, seventy microearthquakes were recorded during the 20-24 September 1976 study. The project was conducted under the Geothermal Exploration Technology Program at the University of California, Lawrence Berkeley Laboratory, which includes investigations of geophysical exploration techniques in different geothermal environments. A similar study of the type described here was conducted at Leach Hot Springs, Grass Valley, Nevada and revealed significant velocity and attenuation anomalies related to the hydrothermal system (Beyer, et al., 1976). Fundamental data in such studies are velocity and attenuation of P and S-waves relative to regional values, as well as source properties and spatial distribution of microearthquakes.

The linear array was placed through the producing steamfield perpendicular to strike of the major geologic trends in the region, as shown in Figure 1. Station 1 and the USGS station SGM served as reference stations to the west and east, respectively, of the present production zone which extends from station 2 through station 12. The boundaries of the geothermal reservoir have not been defined. At the twelve temporary array stations, signals from 4.5 Hz vertical

geophones were radio-telemetered to a central point and recorded, with time and tape speed compensation data, at 0.12 ips on a 14-channel FM tape recorder with 0-40 Hz bandwidth. The thirteenth station, east of the producing field, was a model MEQ-800 portable smoked-paper recorder. Conventional short-period USGS stations in the area provided additional arrival times and first motion data. The locations of the temporary University of California stations are given in Table 1. Based on the results of the 1976 study, to obtain additional wide dynamic range information on magnitudes and source properties of micro-earthquakes, a single channel 12-bit triggered digital casette recorder and a smoked-paper recorder were set out near station 7 in the steam field July 22-25 and August 2-8, 1977. A total of 340 events was recorded on the smoked-paper recorder. The digital recorder malfunctioned during the July period, but 101 events were recorded using a horizontal 4.5 Hz geophone and 54 events were recorded with a similar vertical geophone during the August period.

The goal of this field experiment is an evaluation of the degree to which seismological data of the type considered can provide an indication of water state, porosity, permeability and temperature within a geothermal reservoir, and thus offer a means of delineating field boundaries.

II. EXPLOSION DATA

P-wave Velocities

A fundamental question in this study is whether the presence of the geothermal reservoir is evident in the velocity of propagation of P-waves. A regional reference travel-time curve, shown in Figure

2, with velocities of 5.04 ± 0.10 km/sec and 4.57 ± 0.11 km/sec, was constructed from USGS station readings for both explosions, omitting, however, stations in The Geysers and Clear Lake areas. Data are given in Table 1, elevation corrections are made with respect to station 4 using 4.0 km/sec. These areas can then be compared, for velocity anomalies, to the regional travel-time curve. Explosion travel time data are given in Table 1. The relatively low regional velocities in Figure 2 indicate that only the upper two to three kilometers of the crust are sampled by the first arrivals from the explosions. It was hoped that by recording several regional earthquakes or teleseismic events the deep structure could also be studied. Unfortunately, no such events were recorded during the five-day field period.

Figure 3 presents corrected travel-times for the temporary stations with respect to the regional data in Figure 2. The maximum elevation correction in the field is 128 msec at station 10, yielding a relative time advance of some 200 msec between stations 4 and 10. Slower elevation-correction velocities would increase the relative advances. Stations 1 through 5 plus BKO, PNM, and GYP at 5-10 km distance, appear regionally slightly early for explosion 2, but they are some 150 to over 200 msec late for explosion 1. Along the temporary station array, early arrivals with relative P-wave advances of up to 200 milliseconds are seen commencing around station 5 and continuing to the end of the temporary linear array at station 13. Station SGM to the northeast of the producing field appears regionally normal. USGS Stations SCR, CMT and BGG are also early, i.e., fast with respect to the regional reference model. Station MKI, near Clear Lake, is especially late

for both shots. The general tendency seems to be that times in the production zone and southeast of it are early, and as one proceeds northeastward toward Clear Lake the times become regionally normal, then significantly delayed. This general pattern holds for both the near and far explosions. Close inspection of data from the far explosion reveals that, even though the shape of the curve is the same as that for the near source, the times from the far explosion have been delayed by up to 200 milliseconds with respect to regional. The difference between residuals for the two explosions is a maximum at station 1, indicating the possibility of a low velocity region at intermediate depth (2-4 km) delaying arrivals from the far explosion in that area. The postulated feature coincides with the Mercuryville fault zone, and, possibly with the western edge of the geothermal system.

Attenuation

In addition to the possibility of anomalous velocity, we sought evidence for the production zone affecting the amplitude and waveform of the P-wave. Figure 4 is a record section for explosion 1. It is evident from visual inspection of the first two or three cycles of the P-wave that the waves are attenuated less within the production zone than at station 1, five kilometers west of the production zone.

Two approaches were taken to estimate the attenuation effect at the different sites. The first approach is an adaption of a technique developed by Teng (1968) for analysis of teleseismic data. The ratio of the spectrum of the P-wave at each station to an arbitrary reference station is used to obtain the differential attenuation. Assumptions

are that Q is frequency-independent over the particular frequency band used. The attenuation operator can be expressed as:

$$\exp\left[-\pi f \int_{\text{path}} \frac{ds}{QC} \right]$$

where s = path length

Q^{-1} = intrinsic attenuation = $\frac{2\pi\Delta E}{E}$

$\frac{\Delta E}{E}$ = fraction of strain energy dissipated per cycle

C = P-wave velocity

f = frequency

The path of integration is taken along the ray path. For constant Q the log of the spectral ratio of the P-wave will be a linear function of frequency with slope, $-\pi\delta t/Q$, where δt is the travel-time difference between the two stations. The resulting Q applies to the differential ray path. In practice, one corrects for differences in instrument response and radiation pattern or for any frequency dependent effects which differ at the two stations, and then fits a straight line to the resulting spectral ratio.

An assumption in this method is that the path to both points is the same except over the last fraction of the total path. This results in a negative slope to the spectral ratio, with zero slope for infinite Q, i.e, no attenuation. In practice, positive slopes can be obtained if the path to the first point contains a segment of low Q medium not common to the second path. Widely differing near-surface transfer functions at the two sites can also produce strange effects in the spectral ratio. To minimize such effects it is necessary

to use a smoothed average spectrum as reference in forming ratios. The seismograms from each site for the distant explosion were anti-alias filtered and digitized at 200 samples/sec. The digitized data were then plotted for comparison checks with the analog data to select the proper P-wave intervals. The 0.65 sec P-wave data windows were tapered with a 20% cosine taper, the average signal level was removed, and zeros were added to total 2^{10} points. The data were transformed with a Fast Fourier Transform and corrected for instrument response. Spectra were smoothed with a moving 10-point averaging window. The reduced spectral ratios were then computed and plotted.

The P-waveforms along with individual displacement spectra are shown in the first two columns of Figure 5. Signal-to-noise ratios are maximum in the 2-10 Hz range. The spectra are not corrected for geometrical spreading. The individual spectra show generally less high frequency loss within the production zone. At stations 1 and 12, the spectra have no definite high frequency corner. However, most stations in the geothermal field, e.g., 7 and 8, have well-developed corners at approximately 10 Hz, suggesting higher Q beneath the production zone.

The third column in Figure 5 shows reduced ratios with respect to an averaged spectrum, rather than station 1. Initially, spectral ratios were obtained using station 1 as reference. Examples are shown in Figure 6. In an attempt to reduce the large variations in the ratios, an alternate reference spectrum was sought. The first cycle of the P-wave was analyzed, and its spectrum was smoothed and averaged using all the stations. The resulting average was used as the reference

spectrum. Reduced spectral ratios with respect to this average spectrum are given in the third column of Figure 5. These reduced spectral ratios resemble straight lines. A positive slope to the line means a higher Q than average, a negative slope means a lower Q. Over the entire 1-10 Hz span, stations 1, 2, 6, and 12 exhibit negative slopes while all other sites have positive slopes, indicating a correlation between lower Q at the edges and outside the field, and higher Q within the production zone. Further attempts to use the slopes in Figure 5 for inversion to obtain Q structure would be beyond the quality of the data.

To obtain a more reliable reference spectrum, more stations are needed outside the steam field, but this would have reduced the number of stations over the production zone. The frequency range 3-10 Hz is also susceptible to effects of very shallow structure, rendering difficult the estimation of meaningful spectra. In general, if the data are of sufficient bandwidth and dynamic range, if there are several reference stations outside the zone of interest, and if the target is large enough, then the method of reduced spectral averages can probably be used successfully to delineate anomalous Q zones. The effectiveness might also be increased if longer period P-waves are present in the signal, though the attenuation effects would become small on the scale of this experiment.

A second approach was used to localize the Q variation by considering the amplitude of the first half cycle of the P-wave at each station, specifying more precisely the differential ray paths by using both explosions. The local velocity model shown in Figure 7 was assumed.

We assign to a reference station with first half cycle amplitude A_r, a value Q_r for the vertical part of the path at the station. We can then calculate, based on the model ray path geometry, a value Q_i corresponding to the horizontal propagation path from the reference station to station i and the near-vertical propagation under i, according to

$$Q_i = \pi f \delta t_i / \left[\frac{\pi f \delta t_r}{Q_r} - \alpha \ln \frac{X_i}{X_r} - \ln \frac{A_i}{A_r} \right]$$

where δt_r, δt_i = travel times from a point beneath the reference station to the surface sites

f = apparent frequency of the P-wave

X_r, X_i = source to station distances

α = geometrical attenuation factor, assumed 1.5

The resulting Q_i value will depend on the Q_r assumed, and it will contain information on the entire path from beneath the reference station to the surface at station i. As the Q values obtained are relative and depend on the path assumptions, it is advisable to use a reference station near the region of interest. Results for Q_r values of 30, 45, and 60 for station 2, as reference, are given in Table 2 for both explosions. A maximum value of 250 was assigned to Q_i because the fractional change in amplitude of the wave for higher values of Q cannot be measured over the distance involved.

Resulting Q_i values, with travel time data, are shown in Figure 7 across the field. For both explosions the apparent Q increases throughout the field then decreases again by station 12, for all values of Q_r. This is the same general pattern seen for the spectral ratios. Q values obtained within the field are higher for the more shallow

paths from the near source than for the deeper waves from the far source. Q within the steam field thus appear high with respect to regional values at shallow depths (<1 km), decreasing at greater depths. It is not clear whether the Q values decrease below regional values at depth. Data consistent with high Q in the field come also from the study of the corner frequencies of microearthquakes, discussed in the following section.

III. MICROEARTHQUAKES

Locations

During the five days of recording, seventy earthquakes were observed in the signals monitored for stations 1, 7, and 12. There were no local events recorded by the USGS stations PNM, BKO, SGM, CMT, SCR, BGG, and GYP that were not recorded by the temporary stations. However, there were 12 events recorded by the temporary stations that were recorded only by the two USGS stations closest to the production zone, BKO and CMT, indicating that the microearthquakes are confined to the general area of the steam field. The high rate of seismicity is apparently an ongoing phenomenon. Hamilton and Muffler (1972) recorded 53 events in three weeks with epicenters in the same general area. Lange and Westphal (1969) recorded 19 "small" earthquakes throughout the production zone during a four day observation period. In our later survey, July 22-25 and August 2-8, 1977, 340 events with S-P times less than 1 second were recorded near station 7.

Hypocenters were estimated using a simple regional model of two layers over a halfspace, velocities of 4,5 and 6 km/sec and layer thickness of 1 and 5 km, respectively, obtained by minimizing the

depth standard error in locating several large events at the center of the array using different velocities consistent with the explosion data. Events with clear arrivals on at least five temporary stations and three USGS stations were processed for locations. Forty of the fifty-eight events processed could be located with standard errors less than 0.1 km, indicating fairly well constrained solutions. The epicenters plotted in Figure 8 and location data are listed in Table 3. S-waves were not used in locating the events, but S-wave arrival times were used to estimate Poisson's Ratio, discussed later.

Figure 9 presents the microearthquake hypocenters projected onto the vertical sections shown in Figure 8. The spatial distribution of foci is diffuse, showing no well-defined throughgoing faults. Focal depths are less than 5 km, with an apparent lack of foci in the depth range of 2 to 3 km. Seismicity is also low in the area first exploited for steam, less than 1 km north and northeast of the Geysers Resort. The wells in this area are shallow (less than 1 km) compared to more recent wells, which extend to nearly 3 km. In general, the production zone throughout the field is between two and three km in depth (Richard Dondanville, oral communication, 1977). Most of the larger events, e.g., 28, 29, 45, occurred in an area about 1 km northeast of the Geysers Resort. During the later field study, July 22-25, August 2-8, 1977, a magnitude 2.3 shock was recorded in this same general area.

The temporal distribution of events is also of interest. While clusters of events are seen, there is no indication of systematic migration through the field. For example, events 36, 37, 38, 39,

and 40 occurred within a two hour period but in three separated areas. There were no apparent instances of foreshock activity followed by a main shock, nor of clear aftershock sequences. There were no long aseismic periods; the activity seems to progress at a more or less constant rate.

Mechanisms

P-wave polarities were used in focal mechanism studies. Because complete azimuthal coverage was not obtained, there is ambiguity in the details of fault plane solutions. Only the better constrained solutions are shown on regional fault map in Figure 10. Plotted are the horizontal components of the principal stress axes, mainly compressional in the northeast-southwest direction. This stress is consistent with strike-slip faulting on near-vertical, north-south trending faults, and is typical of regional Coast Range tectonics. Northeast-southwest reverse faulting is also plausible. The northwest trending collayami and north-northwest Konocti Bay fault zones in the Clear Lake volcanics to the northeast are some 20 km long and show right-lateral and vertical movement. Donnelly (1977) states that the small (<1 km lengths) normal faults trending northeast and northwest at Clear Lake are probably the result of crustal adjustments from the extrusion of magma in the region. In the Geysers region the northwest-southeast structural grain is due to the prevailing fault pattern which consists of imbricate reverse faults cut by later strike-slip faults, reflecting the tectonic evolution of the area (McLaughlin and Stanley, 1975).

Magnitudes

Microearthquake magnitudes were otained by averaging coda durations for events recorded at stations 5, 7, 9, and 12. These magnitudes are intended to be equivalent to the local Richter magnitude M_L, in order to compare Geysers earthquake occurrence rates to other central California seismicity. Two different formulae were used for magnitude determination. In the first, $M_{CL} = -0.87 + 2 \log_{10} (T)$ where T is the average coda length from the four stations. The amplitude threshold defining coda length was obtained by comparing measurements for the same events on records from this study with those for the USGS systems with peak magnifications around 15 Hz used by Lee et al., (1972) to develop the M_{CL} scale for central California earthquakes. The second formula $M_{CB} = 0.28 + 0.71 \log_{10} (T)$ was similarly obtained by Bakun and Lindh (1977) for earthquakes with coda lengths less than 30 seconds in the 1975 Oroville, California sequence. If no magnitude is given in Table 3, at least one of the four stations did not have adequate data quality to obtain coda length.

Figure 11 shows the recurrence data fitted to $\log(N) = a-bM$ formulae. b-values of 0.81 ± 0.3 and 2.3 ± 0.15 were found using the M_{CL} and M_{CB} formulae, respectively. A regional b-value of 0.83 ± 0.04 was calculated for 73 events, $2.8 < M_L < 4.8$, occurring within a 50 km radius of The Geysers between 1934 and 1973. C. Bufe (personal communication, 1977) has obtained a b-value of 1.2 for events in the Geysers area with M_{CL} magnitudes between 1 and 3. The M_{CL} derived b-value of 0.8 implies the occurrence of two $M_{CL} = 3$ events per year, and a $M_{CL} = 4$ shock every three years. However, this rate

of occurrence of larger events at The Geysers has not been observed historically. This would indicate that some natural magnitude limiting processing is in operation, that the local b-value is higher than the 0.8 regional value, or that the rate of seismicity is higher now than in recent decades. The M_{CB} recurrence predicts one M_{CB} = 3 event every 600 years, and 121,000 years between M_{CB} = 4 earthquakes. While b = 2.3 is anomalously high, a value somewhat greater than 1 is consistent with the absence of larger events in the area. The magnitude 3.7 earthquake near Cobb Mountain on September 22, 1977, indicates that the 2.3 b-value is too high, if this event is from the population of events in the production zone. This is not clear, but the shock did occur on the edge of the hypothesized steam zone(Geoff et al., 1977).

The application to The Geysers of coda magnitude formulae developed for other regions is a questionable step if occurrence data are to be compared to data for different regions. Coda lengths for several large events and the two explosions varied widely from one USGS station to the next, depending on distance and azimuth. Thus, although the same measurement used routinely by USGS was attempted, it suffered from the unusual variability of earthquake characteristics at The Geysers. The same near-station properties that affect the amplitude of the P-wave will affect the measured coda length. Attenuation appears anomalous in The Geysers, thus our magnitudes and resulting b-values may be meaningless for comparisons to other regions. It is important, but unfortanately difficult, to know if a unique geothermal earthquake exists with occurrence properties different from normal tectonic events.

Because the coda magnitudes are suspect for comparison purposes, we attempted to obtain Wood-Anderson magnitudes (M_L) using data from a single-component 12-bit triggered digital casette recorder and a 4.5 Hz horizontal geophone, set out near station 7 during August 5-8, 1977. One hundred and one events with S-P times less than one second were recorded during the 3-day period. The events were recorded at a sample rate of 200/sec. The digitized time series were Fourier transformed, the instrument response removed, and the resulting spectra of the horizontal ground displacement were conditioned by the Wood-Anderson instrument response

$$\frac{-s^2}{s^2 + 2\delta\omega_n s + \omega_n{}^2}$$

where $s = i\omega$

δ = damping factor = 0.8

ω_n = natural frequency of Wood-Anderson, $\frac{2\pi}{0.8}$ rad/sec.

To avoid noise in the spectra at low and high frequencies, the data were band-limited between 3 and 40 Hz. The equivalent Wood-Anderson spectra were then inverted to the time domain, and the resulting synthetic Wood-Anderson seismograms were read for magnitude M_L in the conventional manner.

Ninety-eight events were processed for Wood-Anderson magnitudes, (Figure 11), resulting in a magnitude range of 0 to 1.8, with a b value of 1.1 ± 0.1, between the two coda b-values of 0.8 and 2.3. The most reasonable estimate of b-value for The Geysers field earthquakes, based on conventional M_L magnitude, is somewhat greater than unity, implying a process producing a higher proportion of small magnitude events

than characteristic of the regional seismicity. As steam is produced and the hydrology altered, the b-values may change with time.

Velocities and Poisson's Ratio

P- to S-wave velocity ratios (V_p/V_s) may be estimated using the Wadati diagram, where S-P time is plotted versus the P-wave arrival time at many different stations for a single event, assuming the same (V_p/V_s) along all propagation paths. The slope of the line through the points is K-1 (where $K = V_p/V_s$). From K, Poisson's Ratio, σ, may be calculated from

$$\sigma = \frac{(K^2-2)}{2(K^2-1)} \quad .$$

This method, which gives an average σ along the paths between the stations and the event, does not require knowledge of the origin time of the earthquake. However, it does require a relatively large number of good S-wave arrivals to obtain a reliable slope. Because horizontal geophones were not used throughout this study, the number of sharp S-wave readings was limited for any particular event. Therefore, we elected to use multiple events at a single station as an alternative method for estimating K-1. This method requires a knowledge of the origin time. However, because the events in this study were located using P times only, and the standard errors were small, it was felt that errors in the origin times would not obscure any significant lateral variation in σ. The method gives a value of Poisson's Ratio along the path to the station for each source, relative to the P-wave velocity used in locating the earthquake. Stations 1, 5, 7, and 12 were selected for analysis using the events grouped as indicated in Table 3, and presented in Figure 12. K-1 was determined by a least

squares fit to the data points constrained to pass through the origin for stations 1, 7, and 12, but through (0.0, 0.1) for station 5, where travel time residuals were consistently between -0.1 and -0.2 sec, while the residuals averaged zero at the stations 1, 7, and 12. Resulting values of σ are 0.15, 0.21, and 0.24 at stations 5, 7, and 12, respectively, while with two different values obtained at station 1, 0.32 using events outside of the field and travel paths not passing through the production zone and 0.27 for events in the center of the field with part of the path through the production zone. This is an indication, thus, of lower values for σ within the production zone, although the data set is limited. Combs and Rotstein (1975) obtained a low Poisson's Ratio of 0.15, at Coso Hot Springs using the same technique. In combination with evidence that the P-wave velocity is higher than regional within the field, the lower Poisson's Ratio implies anomalously high values of the shear modulus within the reservoir. Such a characteristic if real may be related to vapor domination.

Source Parameters

Spectral characteristics of selected events were examined in the search for anomalous features in The Geysers microearthquakes. A difficulty with this approach is the lack of comparative data on the spectral characteristics of microearthquakes in other areas. Douglas et al., (1970) and Douglas and Ryall (1972) have studied Basin and Range events and concluded that scaling laws accepted for large events seem to apply for earthquakes as small as magnitude 1. To allow comparison with other central California areas, Brune's (1970) widely used source model for S-waves, extended to P-waves, was applied.

The parameters of interest are the seismic moment $M_o = 4\pi R\rho V^3 \Omega_o$, the stress drop $\Delta p = (7/16)M_o/r^3$, fault slip $u = M_o/\pi\rho V_s^2 r^2$, and source radius $r = 2.34\ V/f_o 2\pi$, where R = distance from source to receiver, ρ = density (2.67 g/cc), Ω_o = long period displacement spectral level, f_o = corner frequency (f_p or f_s) and V = velocity of material (4.5 km/sec for V_p, 2.6 km/sec for V_s). In addition to source parameter effects such as attenuation, complex propagation path, site response and radiation patterns will affect the spectra. If spectra are averaged for many events or stations, these effects will tend to decrease. The approach is rough but does form a basis for comparing earthquakes. In this study the only correction made to the data was for instrument response, and source parameters were averaged over several stations.

Fourteen events were selected on the basis of magnitude and location within the field. Typical data are shown in Figure 13. Note the wide bandwidth (2-80 hz) recoverable with the digital event recorder. Spectra are shown for the indicated data windows. Corner frequency, f_o, was picked by using Q-corrected templates of the function

$$\left[1 + \left(f/f_o\right)^{2\delta}\right]^{-1/2} \exp(-\pi ft/Q)$$

for travel times t = 0.5, 1.0, 1.5 sec, Q = 40, 80, 120, 250, 700, δ = 3, 5, 7, and f_o = 15, 20, 25, 30, 35, 40, 45, 50, 60 Hz. First the long period level was defined, then each spectrum was fit for f_o, Q, and high frequency roll-off, δ. Results are listed in Table 4a for representative events recorded on the analog system. Tables 4b and 4c present results for P- and S-wave digital data, assuming an average hypocentral distance of 5 km to station 7. (These events

were not located, as the entire network was not operating during the recording period.)

In Figure 14 plots of moment versus magnitude for M_{CL}, M_{CB}, and M_L are presented for the data sets in Table 4. As for b-values, the choice of magnitude alters the results significantly. The results obtained for this study are:

$$\text{Log}_{10}(M_o) = (17.3 \pm 0.1) + (0.8 \pm 0.3)M_{CL}$$

$$\text{Log}_{10}(M_o) = (16.2 \pm 0.3) + (1.9 \pm 0.7)M_{CB}$$

$$\text{Log}_{10}(M_o) = (15.9 \pm 0.03) + (1.3 \pm 0.004)M_L$$

Results from other central California studies of M_o versus M_L are:

Bakun and Bufe (1975), San Andreas:

$$3.5 < M_L < 5$$

$$1 < M_{CL} < 3.5$$

$$\text{Log}_{10}(M_o) = (16.2 \pm 0.1) + (1.52 \pm 0.05)M$$

Bakun and Lindh (1977), Oroville, California

$$17 < \text{Log}_{10}(M_o) < 25$$

$$\text{Log}_{10}(M_o) = (17.02 \pm 0.07) + (1.21 \pm 0.03)M_L$$

Johnson and McEvilly (1974), San Andreas

$$M_L > 2$$

$$\text{Log}_{10}(M_o) = (17.60 \pm 0.28) + (1.16 \pm 0.06)M_L$$

Thatcher and Hanks (1973), Southern California

$$M_L > 3$$

$$\text{Log}_{10}(M_o) = 16.0 + 1.5\ M_L$$

Wyss and Brune (1968), Parkfield, California

$$M_L > 3$$

$$\text{Log}_{10}(M_o) = 17.0 + 1.4\ M_L \quad .$$

From these results it appears that The Geysers events are slightly unusual if the M_L magnitude is used, i.e., for a given M_L, M_o is smaller than for the other relations. In view of these results and the fact that normal b-valves are indicated by the M_L magnitudes from equivalent Wood-Anderson seismograms, it seems that earthquakes at The Geysers are not markedly unusual compared to other central California events. The slightly higher M_L magnitudes may reflect locally low attenuation characteristics.

Corner frequencies are roughly independent of magnitude and moment, implying increasing stress drop with event size if corner frequency is not controlled by Q. However, when a particular event is examined at several different stations, we find that Q must be varied to maintain the same corner frequency. Implied Q values, are given in Table 4a. It was thought that earthquakes beneath the production zone ($h > 3$ km) might exhibit lower corner frequencies (lower Q) than shallow events. Although the highest corner frequency obtained was for a shallow event ($h = 1.7$ km, $f_o = 50$ Hz), there seems to be little correlation between source depth and corner frequency. The Q distribution implied by constraining f_o to be constant at all stations for an event is generally

the same as that indicated by the explosion data; i.e., high in the center of the field, decreasing towards the edges, and lowest outside the major production zone. No variaton with depth can be established.

Because no events were recorded on both vertical and horizontal components, a comparison of Q_p and Q_s cannot be made. Only one station was used in the S-wave study. The S-wave data recorded on the horizontal geophones were thus used only for moment and magnitude determinations and not for a regional Q_s analysis as was done for P-waves.

The majority of events had high frequency spectral slopes, γ, of 3 to 5 and sometimes 7. The corner frequency and high frequency slope depend on the source time-function as well as the source dimensions. The smoother the source function the greater the high frequency roll-off. A source time-function that is relatively smooth in beginning (many continuous derivatives) and ending would produce a much more rapid roll-off than either a sharp explosion or a "chattering" or step-like rupture.

Source function rise-time information, if available in the spectrum, may be useful in determining the materials that are rupturing, the nature of rupture, and the state of stress as well as the source dimensions. Unfortunately, the effects of attenuation are extremely severe at the higher frequencies and almost impossible to remove accurately.

IV. DISCUSSION

Summary of Observations

The significant points observed are:

I. Microearthquakes

(1) High level of activity $0 < M_L < 2$ at 25 to 30 events/day

(2) Distribution in space and time:

(a) shallow foci, < 5 km
(b) no dominant throughgoing faults defined
(c) low seismicity in known steam zones and in original production areas around generating units 1 and 2
(d) slightly higher than normal b-value, using M_L
(e) no systematic pattern to occurrence

(3) Spectral characteristics

(a) slightly anomalous M_o versus M_L relation (low M_o for given M_L)
(b) high corner frequencies, no clear dependence on M_o
(c) f_o for P-waves greater than for S-waves
(d) no relation between f_o and depth
(e) low ($\sim$1 bar) estimated stress drops

(4) Fault plane solutions generally consistent with regional NE-SW compressive stress

II. Velocity Data

(1) Locally high velocity in production region

(2) Broad regionally lower velocity zone extending laterally out of production zone at depth

(3) Apparent low Poisson's Ratio in production zone

III. Attenuation Data

(1) Shallow high Q zone in production zone from explosions and microearthquakes

(2) Deeper lower Q zone from explosions.

A discussion follows of these observations relative to the vapor-dominated reservoir at The Geysers. Implications are investigated, based on known field characteristics, as to possible reflection of reservoir dynamics in the seismological data.

Reservoir Properties

A fundamental question in geothermal exploration is the role of microearthquake data in the detection and delineation of geothermal reservoirs, and in specifying the properties of a reservoir. Earthquake genesis may reflect the steam reservoir properties. The Geysers geothermal field is a vapor dominated reservoir, as opposed to a hot water or brine system characteristic of the Basin and Range or Imperial Valley regions. The temperature and pressure of the vapor region is fairly constant, ranging within a few degrees of 240°C at 30 to 40 bars (Weres, et al., 1977). An unusual characteristic of the reservoir is that the steam is much below expected hydrostatic pressures for the depths involved (2-3 km). Several hypotheses have been advanced to explain the pressure differential. In one, an "incrustation seal" has formed on the edge of the reservoir, inhibiting pressure equalization from surrounding ground water (White, et al., 1971). Minerals such as calcite and anhydrite, whose solubilities decrease with increasing temperature, may reduce permeability at the margins by precipitation from the cooler ground water upon entering the geothermal zone. A similar model proposes an expanding reservoir in which ground water cannot flow rapidly enough into the low pressure steam zone to equalize pressure, by virtue of a high withdrawal rate and adequate heat source to convert pore water into steam. A third explanation calls upon

"traps" of steam, similar to gas traps found in oil producing regions, sealed from surrounding waters.

The dominant rock type in The Geysers reservoir is Franciscan graywacke (McLaughlin and Stanley, 1975), which is initially impermeable and non-porous, but extensively sheared and fractured so that its porosity and permeability is sufficient to provide the existing reservoir. Drill cuttings have shown evidence of secondary porosity from hydrothermal dissolution of minerals (Weres, et al., 1977). In successful steam wells "geothermal sand", alteration products of the minerals, is often encountered above the steam zones (Joe Lafleur, personal communication, 1977). The steam-water interface is probably irregular, reflecting different porosities and capillary effects. The actual amount of economic steam in the reservoir will depend upon the rock type, porosity, permeability, water content and available heat.

An important characteristic of The Geysers reservoir is that it seems to be a maximum enthalpy system. Saturated steam has a maximun enthalpy (heat content) of 2,804 kJ/kg at 234°C and 30 bars. The enthalpies of steam entering boreholes from different units at the Geysers are very near this value (Weres, et al., 1977). Why the steam enthalpy is at this particular value is not entirely clear. However, other steam reservoirs, Lardarello, Italy and Kawah Kamojang, Indonesia also exhibit to some degree the maximum enthalpy phenomenon (Weres, et al., 1977).

Natural leakage, commercial production and interconnected reservoirs are factors proposed to explain the maximum enthalpy phenomenon at The Geysers. Steam flowing toward the wells begins saturated at some temperature above 234°C and is expanded isoenthalpically to less than 30 bars under conditions allowing the water to condense from it. For example, an initially water-saturated isolated reservoir, due to commercial production or surface leakage, would eventually boil dry at temperatures and pressures below 234°C and 30 bars, respectively, depending upon permeability and initial temperature. On the other hand, if there were an unlimited amount of wet steam available from an innerconnected source, the temperature and pressure would stabilize at the maximum enthalpy point. As production continued, steam withdrawn from the 234°C zone would spread, and new wells would develop the maximum enthalpy condition. The actual case is doubtless between unlimited steam and zero steam, which may account for deviation from the maximum enthalpy point.

The state of the reservoir prior to commercial production is not clear. Weres, et al., (1977) hypothesizes that there was a shallow initial vapor zone in the region of units 1 and 2, but as production increased the "deep water table" was boiled down by two or more km to the present 2.5 km. In this "cracked sponge" model water is boiled rapidly from innerconnected cracks; however, there is still a large amount of water left behind in the body of the sponge or in the fine pore structure of the rock, which can serve as a water supply to the steam reservoir. White et al., (1971) suggests a system initially water saturated, but evolving to convection with the introduction

of a potent heat source. Eventually, near-surface temperatures and pressures allow the onset of boiling. Due to limited recharge and permeability, the hot water system becomes a vapor-dominated system. An important aspect of White's model is the recharge area. Because of limited permeability at the incrustation seal, there would be large pressure gradients near the field margins between the reservoir, which is much below hydrostatic pressure, and the exterior of the reservoir, possibly at or above hydrostatic pressure. With increased production the vapor front advances, exposing new regions to pressure differentials. The front would stop advancing when either the heat source was insufficient to cause boiling or the permeability increased so that the recharge and discharge rates balanced.

Seismologically the significant aspects of these reservoir models are: (1) The system is at maximum enthalpy with limited recharge but with extensive fracture permeability, (2) It is low pressure and nearly constant temperature; and (3) It may be expanding at a rate depending upon porosity, permeability and net discharge.

From the concept of differential pressure one would expect microearthquakes to occur where high pore pressures reduce the strength of the materials. The observed locations of microearthquakes appear to concentrate on the margins of the production zone (above and below), where the models would predict the highest pore pressures. Activity is very low, however, above and below the older production zones, implying that the steam source for the older production zone is mainly steam flow from the surrounding reservoir, rather than ground water from above and below. The occurrence of microearthquakes randomly

in time and space also suggests an interconnected geothermal system. The events do not seem to migrate through the field and their pattern suggests no dominant throughgoing faults. The area may be intensely fractured, with the pressure differential activating locally small faults.

Historical data are insufficient to show that microearthquakes are migrating with an expanding reservoir. However, the limited data available do suggest an increasing rate of seismicity. Lange and Westphal (1969) detected a rate of 4 events/day in the fall of 1968. Hamilton and Muffler (1972) recorded a rate of 2-3 events/day in the spring of 1971. At the time of the present study, the power generation rate was 550 Mw or about 7 times the 1971 rate. The microearthquake activity during this study was 25-30 events/day or about ten times the rate observed in previous studies. As this study was conducted in a different manner from previous studies, and because of the short sampling times, it would be difficult to conclude firmly that the microearthquake activity is related to steam withdrawal.

The slightly higher than regional b-value may indicate stress within the microearthquake region. Studies on microfracturing of rock (Scholz, 1968; Wyss, 1973) have shown that b-values depend primarily on the state of stress, and to a lesser extent on the physical properties of the rock. Scholz (1968) found that in a low stress state energy was released in small events, resulting in high b-values. This was particularly true of ductile and high porosity rocks. He also noted that small magnitude events occur in material where crack closing and sliding are important, with the larger events occurring in situations

where new fractures are propagating. While the calculated stress drops are small, it should be realized that due to attenuation it is virtually impossible to obtain a high stress estimate for micro-earthquakes, i.e., corner frequencies of 100 Hz would be associated with stress drops of a few bars at $M_o = 10^{16}$, and corner frequencies cannot be observed at such levels.

The Geysers events are not anomalous compared to regional stresses. Almost all events exhibited strike-slip or dip-slip faulting with the principal compressive stresses in the northeast-southwest direction. It seems plausible that the direction of failure is controlled by regional stress while the rate of failure is controlled by local stress levels.

Thermally induced differential expansion between water in isolated voids and the rock matrix (Knapp and Knight, 1977) is an attractive microearthquake source mechanism from several points of view. Earthquakes would be expected to occur where the permeability is low and the temperature gradient is high, at the edges of the reservoir. In order to produce an event of detectable size, the fracture must coalesce simultaneously over an area of several m^2. Knapp and Knight calculate that, if all the pores fracture at once in a cubic meter of rock with porosity 1%, a zero magnitude event would result. In reality only selected pores fracture, those with preferential orientation with respect to the maximum principal stress. Thermally induced differential expansion may act only as a triggering mechanism for formation of small faults, the maximum size of which would be limited by the scale of variations in rock permeability, porosity and available heat. This failure model would explain an apparent upper magnitude threshold and the higher

than regional b-value. The differential expansion hypothesis is also consistent with the observed fault plane solutions since the model predicts fracture consistent with the direction of the regional stress field.

McGarr (1976) theorized that the volumetric moment, $h\mu|\Delta v|$, is a measure of the amount of seismic failure in response to shear stresses induced by volume change (where μ = shear modulus, $|\Delta v|$ = volume change). Several examples support his theory: volume changes in mining operations, volume changes due to fluid injection (Denver earthquakes), and volume changes associated with uplift (Matsushiro, Japan). An estimate of Δv at The Geysers involves the amount of fluid withdrawn, less groundwater recharge and fluid reinjection. This can be compared to the calculated Δv from the summed moments of the observed seismicity, 1.5×10^{21} to 10^{22} dyne-cm/year, depending on the occurrence used for magnitude 3 events. The larger value (10^{22}), implies Δv of 5×10^{10} cm^3/year, the total volume change necessary to accomplish the observed seismicity, assuming McGarr's model of earthquake genesis. The volume of fluid withdrawn can be calculated from the power generation. At a capacity of 550,000 kw, using a steam rate of 10 kg/kwhr and a specific volume of water of 1.2 cm^3/g, the Δv for 1 year is 5×10^{13} cm^3, some 10^3 times greater than the Δv calculated from the seismicity rate. In other words, McGarr's hypothesis would predict a much higher level of seismicity if the total Δv was consumed by seismic failure. However, the actual Δv available for earthquake generation is much smaller due to ground water recharge and reinjection. A recharge rate equal to discharge would imply no volume change or microearthquakes.

This may explain why seismicity does not change with withdrawal rate in a hot water dominated reservoir that is in hydrostatic equilibrium (Helgeson, 1968; Combs, 1976). Recharge, however, is not instantaneous, nor would one expect the volume change from seismic failure to equal the net volume of water withdrawn. The seismicity may reflect volumetric change in the reservoir, and, if so, the microearthquakes would indicate the regions of expansion of the vapor dominated zone. Temporal change in the spatial pattern of seismicity may occur too slowly to be of practical use. Cessation of events on the edge of the reservoir may indicate an equilibrium situation where the recharge rate is equal to the discharge or the reservoir has expanded to the point where it has been extended beyond a heat source that is sufficient to produce vaporization of available water.

It is not certain whether the steam withdrawal and associated volumetric change is a direct cause of microearthquakes at The Geysers. Because the environment is hydrologically active and because of the intimate relation between fluids and faulting (Hubbert and Ruby, 1959; Nur, 1973), it is probable that fluid withdrawal is a contributing factor. However, only as production increases and expands to areas that are now seismically inactive will we know whether fluid withdrawal is inducing the microearthquakes. Positive correlation would open a new methodology for reservoir modeling, and some consideration should be given to instrumentating new production areas prior to development.

Another failure mechanism which may influence microearthquake activity is "stick-slip" (Brace and Byerlee, 1966) in which the motion occurs in a series of discrete rapid slips. In general, stick-slip

is enhanced by high pressure or normal stresses, low temperature, the presence of strong brittle materials such as feldspars and quartz, the absence of gouge, and lower surface roughness. At higher confining pressures the dominant factor controlling friction strength is effective pressure (Stesky, 1977). In The Geysers reservoir where the temperature is high, and pressure is low, stick-slip would not be expected to dominate. At the reservoir edges where pressures are higher and temperatures are lower, with possible embrittlement due to dehydration (Heard and Ruby, 1965; Raleigh and Paterson, 1965), one would more readily expect stick-slip behavior. The lack of deep events would, in the context of stick-slip earthquakes, imply elevated temperatures beneath the reservoir (4-5 km).

The moment versus magnitude relation for The Geysers, using M_L, results in a low zero-magnitude moment compared to other central California earthquakes. In terms of the seismic waves, for a given moment (low frequency radiation), the amplitude used to determine the magnitude (higher frequency radiation) is larger than for other regions. This is consistent with the high Q observation, but it is difficult to separate source and path effects without dense station coverage.

An indication that source information may be masked by path effects is found in the differences between P-wave and S-wave corner frequencies. P-wave corner frequencies, f_p, are around 30 Hz, and the S-wave corner frequencies, f_s, about 20 Hz. Assuming that fault propagation at a finite rupture velocity controls the observed corner frequencies, and that the rupture velocity is less than the S-wave velocity, then consistent observation of $f_p > f_s$ is incompatible with many faulting

models. In fact, if the fault can be modeled as a long, narrow crack propagating unilaterally, we should observe $f_s > f_p$ over half the radiation pattern. A plausible explanation for the different observed results is the effect of attenuation along the propagation path. A value of Q_s 1/3 to 1/2 that of Q_p would be adequate to produce the observed corner frequencies. If we assume the actual value of f_s at 40 Hz, and that it has been reduced by attenuation to 20 Hz for a travel time, t, of 1.5 seconds for the S-wave, the Q required for the reduction in f_s can be computed from $Q = t/t^*$. $f_s t^*$ of 0.5 is approximately correct for a factor of two reduction in apparent corner frequency (Johnson and McEvilly, 1974, Figure 5). The resulting Q_s, 120, is consistent with the Q_p estimation within the field. This illustrates the extreme difficulty in recovering source parameters such as stress drop or dimensions from microearthquake spectra, even at a distance of 5 km or less.

From the S-wave corner frequencies, calculated stress drops were between 0.1 and 3.0 bar. Because a large number of events at varying azimuths were analyzed, these stress drops are probably representative estimates for the field. The relatively constant values of corner frequency may be indicative of path effects (Q controlled) rather than source effects (time function or dimensions). The larger moment events generally occurred deeper in the field than did smaller events. Assuming uniform detection capability with depth, the larger events would be occurring at depths where the largest pressure differences exist between hydrostatic and the reservoir. The constant corner frequencies can be interpreted as a uniform source dimension of about

50 meters. In a low pressure reservoir with constant permeability and porosity, one would expect uniform source dimensions. Elsewhere in central California, foci are distributed evenly without much correlation between depth and magnitude to depths of 10 to 12 kilometers (McNally, 1976). The fact that earthquakes in The Geysers do not occur deeper than 4 or 5 kilometers is strong evidence for their close association with the geothermal system.

Velocities

The low Poisson's Ratio within the production zone suggested by the microearthquake data may indicate partial saturation of reservoir rocks. Toksoz, Cheng and Timur (1976) found that even a small amount of gas as an immiscible mixture in a brine reduces the compressional wave velocity, V_s, the net effect being a reduced Poisson's Ratio. Nur and Simmons (1969) observed that V_p decreased with decreasing water saturation in low porosity rocks. Both studies would predict the observed low Poisson's Ratio for a vapor dominated reservoir.

As can be seen in Figure 3, there is a P-wave advance (higher velocity) with respect to regional throughout the production zone for shallow propagating waves from the near explosion. For deeper waves from the far explosion, the P-wave velocity appear regionally low, as would be expected within a vapor zone. However, the reduced P-wave velocity is observed over a broad area, much broader than the present production zone. If the presence of steam is controlling the velocity, it would seem that the reservoir is more extensive than presently defined by drill holes. However, P-wave velocity variations in geothermal environments can occur because of structural or stratigraphic

variations. For example a 0.3 second P-wave advance, observed in a Nevada hot springs environment, was clearly due to silica deposition within valley sediments around the hot spring (Beyer, et al., 1976). A similar explanation in terms of compositional differences may apply in the Geysers area. Iyer and Hitcock (1975) observed P-wave delays throughout much of the Clear Lake/Geysers region, and attributed it to a heat source beneath the area. The P-waves from the distant explosion may have been affected by such deeper lower velocity material. Because of the low pressures involved, it is difficult to estimate the temperatures necessary to account for a 10% to 20% velocity decrease.

Lin (1977) from laboratory measurements found for central California rocks about -7×10^{-4} km/sec per degree C velocity change for graywacke and quartz monzonite at pressures greater than 4 kilobars, and about -10^{-3} km/sec per degree C for gabbros. He also found graywacke velocities at room temperature and pressure to vary from 4.8 to 5.7 km/sec with increasing metamorphism. Murase and McBirney (1973) found that for common igneous rocks at 1 bar and less than 600°C there is no change with temperature in seismic velocity. Assuming the dominant material underlying The Geysers to be Franciscan Graywacke with a temperature coefficient for P-wave velocity of -10^{-3}, a decrease in velocity from 5.0 to 4.25 km/sec (15%) at 3 km depth implies an implausible temperature increase of 750°C. It is thus difficult to explain a broad low velocity zone beneath The Geysers by a temperature increase alone.

It appears that the effects of high temperature, degree of water saturation, geologic structure and the compositional change within

the hydrothermal region are combined in producing the observed velocity variations. Detailed studies utilizing distant sources and near vertical propagation through sections will shed light on the regional velocity structure. Results of the present study are clear, however, in the fact that the producing reservoir is characterized by detectably anomalous local seismic wave velocities.

Attenuation

The observed attenuation differences may reflect variations in shallow structure and topography throughout the geothermal field and at reference stations. In a finite element simulation of a ridge with 20^{o} slope, Smith (1975) found that the maximum spectral ratio enhancement was a factor of two at the peak. Data for The Geysers show a factor of 10-20 difference, with little correlation to topography. It is also well known that near-surface effects such as thick, low velocity alluvium can cause amplification, with the degree of enhancement proportional to the contrast in acoustic impedance, and frequencies of the spectral peaks at roughly multiples of the travel time through the superficial layer. There is no evidence for anomalously low velocity shallow materials. For 2 km/sec, the thickness required for enhancement in the 5-10 Hz range would be 100-200 meters. More restrictive, the underlying material would have to be unreasonably high velocity for significant enhancement. Further, the instrument locations were selected to avoid obvious alluvium or landslide surfaces. It is conceivable that bizarre geometrical effects in propagation paths could produce the observed amplitudes. If the actual structure deviates greatly from the model assumed for reducing the data, the observed amplitudes

could reflect focusing. However, the uniformity and spatial extent of the high-Q region argues against such mechanisms. In the formula used for Q estimation, errors in the distance or velocity would need to be an order of magnitude to explain the variations, and this is unlikely. Therefore, the most plausible explanation for the observed amplitude variations is real differences in Q throughout the field.

Johnson et al. (1977) have shown that Q is a function of confining pressure and saturation. He found that both Q_P and Q_S for dry rocks are initially higher and increase much more rapidly with confining pressure than for rocks containing pore water. The effect was attributed to friction and crack closure in the material. Gardner (1964) also showed that Q, as a function of water content alone, increased as the water content decreased. In a theoretical study, White (1975) computed compressional and shear wave velocity and attenuation for partially gas saturated porous rocks. He concluded that for compressional waves the pressure gradients created by a wave traveling through a rock will cause flow of the fluid relative to the rock skeleton and result in attenuation. If the pore-rock matrix is homogenous, the pressure gradients will be small and the attenuation due to fluid flow will also be small. However, if the rock has mixed saturation, such as pockets of gas or partial gas saturation, then the pressure gradients are higher near the inhomogeneities and the loss of energy due to fluid flow will be significant. These effects could explain the shallow high Q zone and the deeper low Q zone at The Geysers. As postulated earlier (Weres et al., 1977), the reservoir may be characterized by a relatively shallow region where the pores are

vapor-dominated. In this region the behavior described by Johnson et al., (1977) and Gardner (1964) may prevail to produce higher Q. Deeper within the reservoir there may be sufficient water for attenuation because of the fluid-flow mechanism of White (1975), thus resulting in the lower Q values. On the other hand, the degree of pore water saturation has opposite effects on P-wave velocity and attenuation. Our data indicate decreases with depth for both parameters within the reservoir, suggesting that water content cannot be the controlling factor for both velocity and attenuation. As for velocity, it would appear that low pressure, temperature, and compositional heterogeneity may contribute, along with water content, to the anomalous attenuation. Temperature effects on attenuation at low pressures, however, can be nonlinear and unpredictable.

V. CONCLUSIONS

The utility of seismological data in the detection and delineation of a geothermal reservoir must depend upon the physical nature of the particular hydrothermal system. There are far too few case histories of geothermal fields to provide even general characteristics of reservoir properties in seismological terms. Nor has it been established unequivocally that there exists such a phenomenon as the 'geothermal earthquake'. Further, there is no compelling evidence that a geothermal reservoir acts as a deep radiator of seismic body waves. It is in such light that observations and conclusions of this study must be viewed, in the context of the low pressure vapor-dominated steam reservoir at The Geysers, as seen with a very limited data base in terms of spatial and temporal sampling.

In terms of regional conditions for central California, The Geysers area appears anomalous to some degree in earthquake occurrence and source parameters, seismic wave velocities, and attenuation properties of the reservoir rocks. Microearthquakes are distributed diffusely, generally absent within the production zone. Depths are less than 5 km. Mechanisms are consistent with NE-SW compressive stress, but no throughgoing faults are indicated. Earthquake occurrence rate suggests a slightly higher than normal b-value, or a seismicity rich in lower magnitude shocks relative to larger events. Both P- and S-wave velocities are higher than regional values in the shallow reservoir; the S-wave velocity, from the low Poisson's Ratio, is even more anomalous than P. Attenuation is low where velocities appear high. There is indication that velocity and attenuation become less anomalous deeper in the field. The anomalous source parameters, low seismic moment for a given magnitude, may be merely a reflection of low attenuation.

It is unfortunate that in this case we cannot say whether these anomalies were present previous to production. The limited observations, along with proposed reservoir models, are consistent with a hypothesis in which the anomalous characteristics are closely related to reservoir depletion. It would be of great value to have such data for a potential geothermal field prior to exploitation.

The microearthquakes may relate to large pressure or temperature gradients, or to volume changes associated with fluid removal. If so, the distribution may delineate the boundary of the steam zone. In several reservoir models this boundary is dynamic, driven by

exploitation of the field, and the resulting seismicity offers promise for monitoring the steam zone configuration.

Source parameters based on high frequency radiation of P- and S-waves, such as fault propagation and dimensions, source rise time and stress drop, suffer in estimation from the high corner frequencies associated with these small events. Even at observation distances of only 5 km or less, and with the high Q values seen in the field, attenuation masks earthquake spectral details at frequencies above 20-30 Hz. Fault plane solutions, based on first motions, generally reflect response to NE-SW compression. More detailed studies may provide information on the fracture mechanisms involved at the field margins.

Anomalously high P- and S-wave velocities and low attenuation characterize the production zone. Extrapolation to in-situ reservoir properties from laboratory and theoretical studies on similar rock types is difficult, thus the mechanisms for the anomalies are not clear. Pressure, temperature, vapor-domination, and chemical alteration must be involved to various degrees.

Clearly our experiment shows that seismological data taken today are useful in delineating the present production zone of The Geysers. Further, the data may offer a means of monitoring the reservoir configuration and properties as these change during exploitation. It is not clear, however, that the same situation would have prevailed prior to major production of the field, and that the same seismological measurements would have been successful at The Geysers in an exploration context.

ACKNOWLEDGMENTS

This research was supported by the U.S. Department of Energy, through the Lawrence Berkeley Laboratory program in Geothermal studies. Special thanks are due personnel of the operating companies at The Geysers field, particularly Mr. Richard Dondanville of Union Oil Company, who provided access to the area for data acquisition.

REFERENCES

Bakun, W. H., and C. G. Bufe, 1975. Shear Wave Attenuation Along the San Andreas Fault Zone in Central California. Bull. Seism. Soc. Amer., v. 65, pp. 439-459.

Bakun, W. H., and A. G. Lindh, 1977. Local Magnitudes, Seismic Moments, and Coda Durations for Earthquakes Near Oroville, California. Bull. Seism. Soc. Amer., v. 67, pp. 615-629.

Beyer, H., A. Dey, A. Liaw, E. Majer, T. V. McEvilly, H. F. Morrison, and H. Wollenberg, 1976. Preliminary Open File Report Geological and Geophysical Studies in Grass Valley, Nevada. Lawrence Berkeley Laboratory Report, LBL-5262.

Brace, W. F., and J. D. Byerlee, 1966. Stick-slip as a Mechanism for Earthquakes. Science, v. 153, p. 990.

Brune, J. N., 1970. Tectonic Stress and the Spectra of Seismic Shear Waves From Earthquakes. J. Geophys. Research, v. 75, pp. 4997-5009.

Brune, J. N., 1971. Correction (to Brune 1970). J. Geophys. Research, v. 76, p. 5002.

Combs, J., 1976. Microearthquake Studies Before and During Fluid Withdrawal and Reinjection Test, East Mesa Geothermal Field, Imperial County, California. Contribution #7-77, Center for Energy Studies, University of Texas at Dallas.

Combs, J. and Y. Rostein, 1975. Microearthquake Studies at the Coso Geothermal Area, China Lake, California. 2nd U.N. Symp. on the Dev. and Use of Geothermal Resources, San Francisco, pp. 909-916.

Donnelly, J. M., 1977. Geochronology and Evolution of the Clear Lake Volcanic Field. Ph.D. Thesis, University of California, Berkeley.

Douglas, B. M. and A. Ryall, 1972. Spectral Characteristics and Stress Drop for Microearthquakes Near Fairview Peak, Nevada. J. Geophys. Research, v. 77, pp. 351-359.

Douglas, B. M., A. Ryall, and R. Williams, 1970. Specral Characteristics of Central Nevada Microearthquakes. Bull. Seism. Soc., Amer., v. 60, pp. 1547-1559.

Gardner, G. H. F., M. R. J. Wyllie, and D. M. Droschak, 1964. Effects of Pressure and Fluid Saturation on the Attenuation of Elastic Waves in Sands. J. Petroleum Tech., v. 16, pp. 189-198.

Goff, F. E., J. M. Donnelly, and B. C. Hearn, 1977. Geothermal Prospecting in The Geysers - Clear Lake Area, Northern California. Geology, v. 5, pp. 509-515.

Hamilton, R. M., and L. J. P. Muffler, 1972. Microearthquakes at The Geysers Geothermal Area, California. J. Geophy. Research, v. 77, pp. 2081-2086.

Heard, H. C., and W. W. Rubey, 1966. Tectonic Implications of Gypsum Dehydration. Geo. Soc. of Amer. Bull., v. 77, pp. 741-760.

Helgeson, H. C., 1968. Geologic and Thermodynamic Characteristics of the Salton Sea Geothermal System. Amer. J. of Science, v. 2(66), pp. 129-166.

Hubbert, M. K., and W. W. Rubey, Role of Fluid Pressure in Mechanics of Overthrust Faultings. Bull. Geol. Soc. Amer., v. 70, pp. 115-166.

Iyer, H. M., and T. Hitchcock, 1975. Teleseismic Residuals at The Geysers Geothemal Area. Amer. Geophys. Union Trans., v. 56, p. 1020.

James, R., 1968. Wairakei and Lardarello: Geothermal Power Systems Compared. New Zealand Journal of Science, v. 11, pp. 706-719.

Johnson, L. R., and T. V. McEvilly, 1974. Near-field Observations and Source Parameters of Central California Earthquakes. Bull. Seism. Soc. Amer., v. 64, pp. 1855-1886.

Johnson, D. H., M. N. Toksoz, and A. Timer, 1977. Attenuation of Seismic Waves in Dry and Saturated Rocks. II: Mechanisms. in press.

Knapp, R. B., and J. E. Knight, 1977. Differential Thermal Explosion of Pore Fields: Fracture Propagation and Microearthquake Production in Hot Pluton Environments. J. Geophys. Research, v. 82, pp. 2515-2522.

Lange, A. L., and W. H. Westphal, 1969. Microearthquakes Near The Geysers, Sonoma County, California. J. Geophys. Research, v. 74, pp. 4377-4382.

Lee, W. H. K., Bennett, R. E., Meagher, K. L., 1972. A Method of Estimating Magnitude of Local Earthquakes From Signal Duration. USGS open file report.

Lin, W., 1977. Velocities of Compressional Wave in Rocks of Central California at High Pressure and High Temperature and Applications to the Study of the Crustal Structure of California Coast Ranges. Ph.D. Thesis, University of California, Berkeley.

McGarr, A., 1976. Seismic Moments and Volume Change. J. Geophys. Research, v. 81, pp. 1487-1494.

McLaughlin, R. J. and W. D. Stanley, 1975. Pre-tertiary Geology and Structural Control of Geothermal Resources, The Geysers Steam Field, California. 2nd U.N. Symposium on the Development and Use of Geothermal Resources, San Francisco, California, pp. 475-485.

McNally, K. C., 1976. Spatial, Temporal, and Mechanistic Character in Earthquake Occurrence. A Segment of the San Andreas Fault in Central California. Ph.D. Thesis, University of California, Berkeley.

Murase, T., and A. R. McBirney, 1973. Properties of Some Common Igneous Rocks and Their Melts at High Temperature. Bull. Geo. Soc. Amer., v. 84, pp. 3563-3592.

Nur, A., 1973. Role of Pure Fluids in Faulting. Phil Trans. R. Soc. Lond., v. 274, pp. 297-304.

Nur, A., and G. Simmons, 1969. The Effect of Saturation on Velocity in Low Porosity Rocks. Earth Plan. Sci. Letters, v. 7, pp. 183-193.

Raleigh, C. B., and M. S. Paterson, 1965. Experimental Deformation of Serpentinite the Its Tectonic Implications. J. Geophy. Research, v. 70, pp. 3965-3985.

Scholz, C. H., 1968. The Frequency-Magnitude Relation of Microfracturing in Rock and Its Relation to Earthquakes. Bull. Seis. Soc. Amer., v. 58, pp. 399-415.

Smith, W. D., 1975. A Finie Element Study of the Effects of Structural Irregularities on Body Wave Propagation. Ph.D. Thesis, University of California, Berkeley.

Stesky, R. M., 1977. Rock Friction - Effect of Confining Pressure. Proc. of Conference II Experimental Studies of Rock Friction With Application to Earthquake Prediction. U.S.G.S., pp. 331-353.

Teng, T., 196 . Attenuation of Body Waves and the Q Structure of the Mantle: J. Geophy. Research, v. 73, pp. 2195-2216.

Thatcher, W. and T. C. Hanks, 1973. Source Parameters of Southern California Earthquakes, J. Geophy. Research, v. 77, pp. 1549-1565.

Toksoz, M. N., C. H. Cheng, and A. Timur, 1976. Velocities of Seismic Waves in Porous Rocks. Geophysics, v. 41, pp. 621-645.

Weres, O., K. Tsao, and B. Wood, 1977. Resource Technology and Environment at The Geysers. Lawrence Berkeley Laboratory, LBL-5231.

White, D. E., L. J. P. Muffler, and A. H. Truesdell, 1971. Vapor-dominated Hydrothermal Systems Compared with Hot-Water Systems. Economic Geology, v. 66, pp. 75-97.

White, J. E., 1975. Computed Seismic Speeds and Attenuation in Rocks With Partial Gas Saturation. Geophysics, v. 40, pp. 224-232.

Wyss, M., 1973. Towards a Physical Understanding of the Earthquake Frequency Distribution. Geophys. J. R. Astr. Soc., v. 31, pp. 341-359.

Wyss, M., and J. N. Brune, 1968. Seismic Moment, Stress, and Source Dimensions for Earthquakes in the California-Nevada Region. J. Geophys. Research, v. 73, pp. 4681-4694.

Table 1. Station and Explosion Data

Station	Latitude (N)	Longitude (W)	Elev. (m)	Explosion #1 Travel Time Corrected/Residual	Explosion #2 Travel Time Corrected/Residual
1	38° 47.124'	122° 52.692'	746	3.523 / +.222	1.183 / -.090
2	38° 47.847'	122° 50.258'	736	4.212 / +.200	1.835 / -.052
3	38° 48.100'	122° 50.109'	567	4.260 / +.160	1.872 / -.050
4	38° 48.210'	122° 49.845'	476	4.320 / +.134	1.940 / -.050
5	38° 48.483'	122° 49.296'	552	4.586 / +.135	2.091 / -.066
6	38° 48.653'	122° 49.000'	692	4.566 / +.088	2.146 / -.110
7	38° 48.669'	122° 48.639'	731	4.619 / +.047	2.231 / -.136
8	38° 48.840'	122° 48.532'	889	4.644 / +.015	2.246 / -.165
9	38° 48.891'	122° 48.193'	950	4.698 / -.036	2.311 / -.211
10	38° 48.788'	122° 47.735'	988	4.770 / -.060	2.432 / -.240
11	38° 49.045'	122° 47.456'	882	4.882 / -.050	2.528 / -.220
12	38° 49.474'	122° 46.639'	1050	5.159 / -.075	2.826 / -.203
13	38° 50.578'	122° 45.662'	721	-- / --	3.21 / -.21
*BRO	38° 49.46'	122° 50.57'	879	4.35 / +.14	1.68 / -.08
*PNM	38° 50.85'	122° 56.78'	783	3.62 / +.14	1.07 / -.06
*GYP	38° 45.88'	122° 50.65'	1054	3.77 / +.05	2.05 / -.03
*SKG	38° 42.12'	123° 00.81'	282	0.84 / +.08	3.45 / +.200
GLV	38° 53.80'	122° 46.58'	893	6.25 / -.11	3.65 / -.07

Table 1. Station and Explosion Data (cont)

Station	Latitude (N)	Longitude (W)	Elev. (m)	Explosion #1 Travel Time Corrected/Residual	Explosion #2 Travel Time Corrected/Residual
SGM	38° 52.03'	122° 42.58'	1080	6.85 / +.17	4.29 / -.08
BGG	38° 48.84'	122 40.76'	1125	6.46 / -.24	4.39 / -.32
CMT	38° 48.35'	122° 45.31'	1284	5.14 / -.26	3.01 / -.42
SCR	38° 46.15'	122° 46.87'	1015	4.65 / -.08	2.79 / -.32
*MWS	38° 33.03'	122° 43.37'	144	7.15 / +.01	7.05 / +.16
*FTR	38° 31.36'	123° 09.66'	528	5.48 / +.02	7.84 / -.09
*HLB	38° 35.36'	122° 54.54'	165	4.05 / +.02	5.34 / +.03
*MOF	38° 42.61'	123° 08.59'	803	2.43 / -.02	4.72 / -.04
*MCL	38° 47.56'	123° 07.80'	428	2.83 / +.06	3.93 / -.01
*DRY	38° 46.03'	123° 14.31'	772	4.25 / 0.	5.92 / +.03
*SNO	38° 56.43'	123° 11.50'	870	5.92 / -.08	5.80 / -.07
MKI	38° 58.17'	122° 47.22'	905	7.60 / +.42	4.89 / +.21
*BDC	38° 36,36'	123° 11.81'	518	4.40 / 0.0	

*Station used for velocity model

Explosion Locations and Origin Times

	Time (UTC)		Location	
#1	1235 00.58	Day 266	38°43.50'N	123°01.44'W
#2	1235 00.64	Day 268	38°48.60'N	122°55.62'W

Table 2

Average Attenuation Values, Q_i, for various Q_r, for Explosions 1, 2 respectively

Station	Q_r = 30	Q_r = 45	Q_r = 60
1	14,10	17,12	19,13
2	30,30	45,45	60,60
3	33,32	52,51	71,67
4	38,--	63,--	94,--
5	48,--	86,--	142,--
6	44,75	71,189	102,250
7	41,164	63,250	86,250
8	34,92	47,250	58,250
9	28,50	36,76	43,94
10	30,62	37,100	44,132
11	40,34	56,42	70,47
12	19,51	23,66	25,75

Table 3
Microearthquake Locations

Sequence Number	M_{CB}	M_{CL}	Latitude	Longitude	Depth (km)	S.E. of Epicenter (km)	σ group
1			38°48.54'N	122°48.06'W	0.71	.02	
2	0.6	0.1					
3	0.4	-0.5	48.58'	48.86'	1.19	.07	5,12
4			48.35'	48.37'	2.79	.01	
5	0.2	-1.0	49.18'	48.26'	0.84	.05	5,12
6	0.4	-0.6	48.32'	47.70'	1.41	.03	
7	0.7	0.2	47.57'	48.25'	4.40	.07	1,5
8	0.2	-1.0	48.17'	48.93'	0.90	.10	
9	0.7	0.2	48.46'	48.16'	0.75	.07	
10	0.1	-1.3					
11	0.5	-0.4					
12	0.8	0.5					
13	0.4	-0.6					
14	0.1	-1.3	48.94'	49.06'	1.43	.07	7,12
15	0.4	-0.6	49.24'	48.25'	1.74	.03	5
16	0.4	-0.5	48.86'	48.82	1.58	.05	12
17	0.3	-0.7	48.84'	48.94'	1.49	.08	12
18	0.3	-0.9	48,89'	49.04'	1.30	.07	12
19	0.3	-0.9	49.06'	48.95'	1.41	.04	5
20	0.3	-0.7					
21	0.3	-0.8	48.98'	48.95'	1.54	.03	12
22	0.2	-1.2					12
23	0.3	-0.7	47.57'	48.34'	3.0	.05	5,12
24	0.3	-0.9	48.53'	49.50'	1.11	.01	5,7
25	0.6	0.1	48.36'	47.86'	4.14	.5	7
26	0.4	-0.5	47.56'	48.50'	3.0	.06	
27	0.4	-0.4	49.01'	49.84'	0.67	.09	1
28	0.7	0.3	48.51'	47.97'	3.55	.05	1
29	0.9	0.9	48.66'	47.80'	3.76	.05	1
30	0.8	0.8	48.97'	48.86'	1.25	.03	12
32	0.3	-0.8	49.05'	48.74'	0.60	.03	
33	0.4	-0.6					
34	0.7	0.1	48.78'	48.10'	1.64	.04	7
35	0.5	-0.2	48.63'	48.55'	3.70	.08	12
36			49.01'	48.84'	1.38	.04	12
37			48.37'	46.74'	3.77	.09	12
38	0.3	-0.8	48.50'	48.16'	2.86	.10	
39	0.4	-0.4	48.11'	46.54	1.64	.07	7,12
40	0.6	0	48.09'	46.49'	0.52	.10	7,12
41	0.3	-0.7	48.65	48.18'	3.18	.03	
42	0.7	0.2	48.93'	48.34'	3.75	.06	1
44	0.5	-0.3					
45	1.0	1.2	48.39'	47.81'	3.05	.05	5
46	0.5	-0.3					
47	0.2	-1.1					
48	0.3	-0.9					
49	0.4	-0.6	48.21'	49.17'	1.92	.04	1
50	0.7	0.3	47.90'	48.92'	0.40	.05	1,5
51	0.5	-0.1	48.88'	48.09'	3.50	.05	7
52	0.5	-0.1	49.01'	48.97'	0.98	.07	12
53	0.4	-0.5					
57			48.48'	47.95'	3.59	.04	
58	0.5	-0.3	48.80'	48.06'	4.01	.07	7

Table 4

a) P-wave Spectral Parameters (Analog FM System)

Event	STA	R (km)	M_o (dyne-cm)	Q	f_o (Hz)	δ	Depth (km)	ΔP (bar)	u (cm)	r (m)
3	7	1.3	1.2×10^{17}	250						
3	11	2.5	1.7×10^{17}	120	25	5	1.2	0.23	2.02×10^{-3}	66
3	12	3.8	1.9×10^{17}	80						
37	7	4.7	1.3×10^{17}	250						
37	3	6.3	3.8×10^{17}		25	3	3.8	0.25	2.27×10^{-3}	66
37	11	4.1	1.5×10^{17}	250						
37	12	4.3	1.3×10^{16}	120						
39	7	3.6	6.4×10^{16}	250						
39	3	5.1	6.1×10^{16}	120	35	3	1.6	0.13	9.32×10^{-3}	47
39	11	2.7	1.6×10^{16}	80						
39	12	3.0	1.3×10^{16}	40						
42	7	3.8	3.4×10^{17}	250						
42	3	3.9	4.1×10^{17}	120						
42	11	4.0	3.5×10^{17}	120	25	5	3.8	0.48	4.32×10^{-3}	66
42	12	4.6	2.7×10^{17}	80						
42	1	8.0	2.6×10^{17}	60						
41	7	3.3	7.8×10^{16}	250						
41	3	4.1	4.8×10^{16}	120	30	3	3.2	0.14	1.01×10^{-3}	55
41	11	3.5	4.6×10^{16}	120						
41	12	4.2	3.7×10^{16}	40						
51	7	3.6	1.4×10^{17}	250						
51	3	4.5	1.7×10^{17}	120						
51	11	3.6	1.5×10^{17}	120	35	5	3.5	0.63	3.46×10^{-3}	47
51	12	4.2	1.3×10^{17}	40						
51	1	8.2	9.7×10^{16}	40						
7	7	4.8	2.0×10^{17}	250	30	7	4.4	0.52	3.89×10^{-3}	55
15	7	2.1	7.9×10^{16}	250	50	5	1.7	0.96	4.27×10^{-3}	33
17	7	1.6	1.0×10^{17}	250	30	7	1.5	0.26	1.94×10^{-3}	55
18	7	1.5	7.9×10^{16}	250	35	3	1.3	0.33	2.11×10^{-3}	47
28	7	3.7	4.0×10^{17}	250	25	5	3.6	0.61	5.41×10^{-3}	66
34	7	1.8	1.3×10^{17}	250	35	5	1.6	0.54	1.75×10^{-3}	47
38	7	3.0	1.0×10^{17}	250	25	7	2.9	0.15	1.35×10^{-3}	66
58	7	4.1	3.2×10^{17}	250	25	5	4.0	0.49	4.32×10^{-3}	66

Table 4 (Cont.)

b) P-wave Spectral Parameters (Digital System)

$\bar{R}$ = 5.0 km		STATION 7		
M_o (dyne-cm)	f_o (Hz)	ΔP (bar)	u (cm)	r (m)
1.6×10^{17}	40	1.02	5.6×10^{-3}	41
3.7×10^{16}	40	0.23	1.3×10^{-3}	41
2.1×10^{17}	20	0.17	1.8×10^{-3}	82
2.1×10^{17}	20	0.17	1.8×10^{-3}	82
1.6×10^{17}	25	0.24	2.2×10^{-3}	66
2.6×10^{16}	35	0.19	6.9×10^{-4}	47
8.5×10^{16}	40	0.54	2.9×10^{-3}	41
6.3×10^{16}	40	0.40	2.2×10^{-3}	41
8.5×10^{16}	35	0.36	2.3×10^{-3}	47
2.4×10^{16}	40	0.15	8.4×10^{-4}	41
5.3×10^{16}	40	0.33	1.9×10^{-3}	41

Table 4 (Cont.)

c) S-wave Spectral Parameters (Digital System)

$\bar{R}$ = 5.0 km STATION = 7

M_L	M_o (dyne-cm)	f_o (Hz)	ΔP (bar)	u (cm)	r (m)
0.6	4.1×10^{16}	25	3.0×10^{-1}	4.8×10^{-3}	38
0.3	1.2×10^{16}	25	9.2×10^{-2}	1.4×10^{-3}	38
0.9	7.1×10^{16}	25	5.4×10^{-1}	8.4×10^{-3}	38
0.5	2.0×10^{16}	25	1.5×10^{-1}	2.4×10^{-3}	38
0.4	1.6×10^{16}	25	1.2×10^{-1}	1.9×10^{-3}	38
1.6	1.2×10^{18}	35	2.5×10^{1}	2.8×10^{-1}	27
1.6	4.1×10^{17}	20	1.5×10^{0}	3.1×10^{-2}	48
0.9	6.1×10^{16}	25	4.6×10^{-1}	7.2×10^{-3}	38
0.4	2.0×10^{16}	25	1.5×10^{-1}	2.4×10^{-3}	38
0.5	2.0×10^{16}	30	2.6×10^{-1}	3.4×10^{-3}	32
1.4	3.0×10^{17}	25	2.3×10^{0}	3.6×10^{-2}	38
0.8	1.2×10^{17}	15	2.0×10^{-1}	5.2×10^{-3}	64
1.1	1.8×10^{17}	25	1.3×10^{0}	2.1×10^{-2}	38
0.4	3.0×10^{16}	25	2.3×10^{-1}	3.6×10^{-3}	38
0.3	1.4×10^{16}	20	5.5×10^{-2}	1.0×10^{-3}	48
0.2	1.8×10^{16}	25	1.3×10^{-1}	2.1×10^{-3}	38
0.6	6.1×10^{16}	20	2.3×10^{-1}	4.6×10^{-3}	48
1.1	1.2×10^{17}	25	9.2×10^{-1}	1.4x10-2	38
0.3	2.0×10^{16}	25	1.5×10^{-1}	2.4×10^{-3}	38
0.0	2.4×10^{15}	15	4.0×10^{-3}	1.0×10^{-4}	64
0.3	1.8×10^{16}	20	7.1×10^{-2}	1.4×10^{-3}	48

Table 4 (Cont.)

c) S-wave spectral Parameters (Digital System)

$\bar{R}$ = 5.0 km STATION = 7

M_L	M_o (dyne-cm)	f_o (Hz)	ΔP (bar)	u (cm)	r (m)
1.4	3.0×10^{17}	20	1.1×10^{0}	2.3×10^{-2}	48
0.5	3.2×10^{16}	25	2.4×10^{-1}	3.8×10^{-3}	38
0.6	4.1×10^{16}	25	3.0×10^{-1}	4.8×10^{-3}	38
0.4	2.0×10^{16}	20	7.9×10^{-2}	1.5×10^{-3}	48
0.6	6.1×10^{16}	15	1.0×10^{-1}	2.6×10^{-3}	64
0.4	4.1×10^{16}	20	1.5×10^{-1}	3.1×10^{-3}	48
1.1	4.1×10^{17}	15	6.6×10^{-1}	1.7×10^{-2}	64
0.4	3.0×10^{16}	25	2.3×10^{-1}	3.6×10^{-3}	38
1.3	3.0×10^{17}	15	5.0×10^{-1}	1.3×10^{-2}	64
1.2	1.8×10^{17}	20	7.1×10^{-1}	1.4×10^{-2}	48
0.2	1.2×10^{16}	20	4.7×10^{-2}	9.3×10^{-4}	48
0.1	9.2×10^{15}	20	3.5×10^{-2}	6.9×10^{-4}	48
1.7	1.2×10^{18}	15	2.0×10^{0}	5.2×10^{-2}	64
0.4	3.0×10^{16}	25	2.3×10^{-1}	3.6×10^{-3}	38
0.6	4.1×10^{16}	30	5.3×10^{-1}	6.9×10^{-3}	32
1.4	2.4×10^{17}	20	9.4×10^{-1}	1.8×10^{-2}	48
0.5	4.1×10^{16}	25	3.0×10^{-1}	4.8×10^{-3}	38
0.6	4.1×10^{16}	20	1.5×10^{-1}	3.1×10^{-3}	48
0.2	1.6×10^{16}	30	2.1×10^{-1}	2.8×10^{-3}	32
0.3	1.8×10^{16}	25	1.3×10^{-1}	2.1×10^{-3}	38
0.5	3.0×10^{16}	25	2.3×10^{-1}	3.6×10^{-3}	38

Table 4 (Cont.)

c) S-wave spectral Parameters (Digital System)

$\bar{R}$ = 5.0 km STATION = 7

M_L	M_o (dyne-cm)	f_o (Hz)	ΔP (bar)	u (cm)	r (m)
0.5	1.6×10^{17}	20	6.3×10^{-1}	1.2×10^{-2}	48
0.4	1.8×10^{16}	25	1.3×10^{-1}	2.1×10^{-3}	38
0.1	1.4×10^{16}	25	1.0×10^{-1}	1.7×10^{-3}	38
0.8	6.1×10^{16}	25	4.6×10^{-1}	7.2×10^{-3}	38
1.0	1.4×10^{17}	20	5.5×10^{-1}	1.0×10^{-2}	48
0.8	1.2×10^{17}	15	2.0×10^{-1}	5.2×10^{-3}	64
0.1	8.1×10^{15}	30	1.0×10^{-1}	1.4×10^{-3}	32
0.8	1.2×10^{17}	20	3.9×10^{-1}	7.7×10^{-3}	48
1.3	3.0×10^{17}	25	2.3×10^{0}	3.6×10^{-2}	38
1.5	5.1×10^{17}	20	1.9×10^{0}	3.8×10^{-2}	48
0.9	1.2×10^{17}	20	4.7×10^{-1}	9.3×10^{-3}	48
1.3	2.0×10^{17}	15	3.3×10^{-1}	8.7×10^{-3}	64
0.7	1.0×10^{17}	20	3.9×10^{-1}	7.7×10^{-3}	48
1.2	3.0×10^{17}	20	1.1×10^{0}	2.3×10^{-2}	48
1.0	1.4×10^{17}	20	5.5×10^{-1}	1.0×10^{-2}	48
1.2	2.0×10^{17}	20	7.9×10^{-1}	1.5×10^{-2}	48
0.4	1.6×10^{16}	25	1.2×10^{-1}	1.9×10^{-3}	38
0.9	1.0×10^{17}	20	3.9×10^{-1}	7.7×10^{-3}	48
0.0	4.1×10^{15}	35	8.4×10^{-2}	9.5×10^{-4}	27
1.7	1.0×10^{18}	15	1.6×10^{0}	4.3×10^{-2}	64
0.8	8.1×10^{16}	25	6.1×10^{-1}	9.7×10^{-3}	38

Table 4 (Cont.)

c) S-wave spectral Parameters (Digital System)

$\bar{R}$ = 5.0 km STATION = 7

M_L	M_o (dyne-cm)	f_o (Hz)	ΔP (bar)	u (cm)	r (m)
0.7	8.1×10^{16}	26	6.1×10^{-1}	9.7×10^{-3}	38
0.6	5.1×10^{16}	15	8.3×10^{-2}	2.1×10^{-3}	64
0.2	7.1×10^{15}	20	2.7×10^{-2}	5.4×10^{-4}	48
0.1	5.1×10^{15}	25	3.8×10^{-2}	6.0×10^{-4}	38
0.5	4.1×10^{16}	10	1.9×10^{-2}	7.7×10^{-4}	96
0.4	3.0×10^{16}	15	5.0×10^{-2}	1.3×10^{-3}	64
0.2	1.2×10^{16}	25	9.2×10^{-2}	1.4×10^{-3}	38
0.5	5.1×10^{16}	25	3.8×10^{-1}	6.0×10^{-3}	38
0.6	7.1×10^{16}	25	5.4×10^{-1}	8.4×10^{-3}	38
1.0	1.8×10^{17}	20	7.1×10^{-1}	1.4×10^{-2}	48
0.2	5.1×10^{15}	35	1.0×10^{-1}	1.1×10^{-3}	27
0.7	8.1×10^{16}	25	6.1×10^{-1}	9.7×10^{-3}	38
0.3	1.5×10^{16}	30	2.0×10^{-1}	2.6×10^{-3}	32
1.2	2.0×10^{17}	15	3.3×10^{-1}	8.7×10^{-3}	64
0.4	1.6×10^{16}	25	1.2×10^{-1}	1.9×10^{-3}	38
0.4	1.4×10^{16}	30	1.8×10^{-1}	2.4×10^{-3}	32
1.8	1.6×10^{18}	10	7.9×10^{-1}	3.1×10^{-2}	96
0.3	1.4×10^{16}	25	1.0×10^{-1}	1.7×10^{-3}	38
0.3	1.4×10^{16}	25	1.0×10^{-1}	1.7×10^{-3}	38
0.7	7.1×10^{16}	25	5.4×10^{-1}	8.4×10^{-3}	38

Table 4 (Cont.)

c) S-wave spectral Parameters (Digital System)

$\bar{R}$ = 5.0 km STATION = 7

M_L	M_o (dyne-cm)	f_o (Hz)	ΔP (bar)	u (cm)	r (m)
0.7	1.0×10^{17}	15	1.6×10^{-1}	4.3×10^{-3}	64
0.3	1.8×10^{16}	25	1.3×10^{-1}	2.1×10^{-3}	38
0.7	5.1×10^{16}	25	3.8×10^{-1}	6.0×10^{-3}	38
0.5	3.0×10^{16}	30	4.0×10^{-1}	5.2×10^{-3}	32
0.2	1.0×10^{16}	25	7.7×10^{-2}	1.2×10^{-3}	38
0.5	3.0×10^{16}	15	5.0×10^{-2}	1.3×10^{-3}	64
0.6	3.0×10^{16}	25	2.3×10^{-1}	3.6×10^{-3}	38
0.5	5.1×10^{16}	15	8.3×10^{-2}	2.1×10^{-3}	64
0.4	3.2×10^{16}	30	4.2×10^{-1}	5.5×10^{-3}	32
0.9	1.8×10^{18}	15	3.0×10^{-1}	7.8×10^{-3}	64
1.8	1.2×10^{18}	25	9.2×10^{0}	1.4×10^{-1}	38
1.1	1.6×10^{17}	25	1.2×10^{0}	1.9×10^{-2}	38
0.2	8.1×10^{15}	25	6.1×10^{-2}	9.7×10^{-4}	38
0.2	1.2×10^{16}	25	9.2×10^{-2}	1.4×10^{-3}	38
0.6	5.1×10^{16}	25	3.8×10^{-1}	6.0×10^{-3}	38

FIGURE CAPTIONS

Figure 1. Permanent (USGS) seismographic stations in the Geysers - Clear Lake area, and temporary (Berkeley) station array in the geothermal field. Box indicates area in subsequent maps. Refraction explosion locations are shown.

Figure 2. Regional travel-times for stations outside known geothermal area, based on the two explosions, corrected for elevations.

Figure 3. Reduced travel-times, with respect to velocities shown in Figure 2, for stations within The Geysers - Clear Lake area, for both explosions. Temporary stations are numbered, USGS stations are shown by name.

Figure 4. Seismograms from the far explosion, plotted at equal gains and at relative distances.

Figure 5. P-wave signals, spectra, and spectral ratios with respect to smoothed reference spectrum (see text).

Figure 6. Example spectral ratios with respect to station 1 spectrum, unsmoothed, as reference.

Figure 7. Composite model for Q estimation, showing P-wave travel-time residuals and Q_i through the production zone for both explosions. Zone of inferred high Q and high velocity is shaded. Q_r is assumed to be 60.

Figure 8. Epicenters, with sequence numbers (see Table 3), for well-located microearthquakes recorded 20-24 September, 1976. Sections in Figure 9 are indicated.

Figure 9. Cross sections of hypocenters through the steam production zone. Section lines are shown in Figure 8.

Figure 10. Horizontal projections of principal stress axes from fault-plane solutions. Either compression or tension axis is given, whichever is near-horizontal. Faults adapted from McLaughlin, 1974.

Figure 11. Microearthquake occurrence data based on different magnitude formulae. M_{CL} and M_{CB} are coda-length magnitudes for the same 1976 data set (4 days). M_L is equivalent Wood-Anderson magnitude for the August, 1977 data set (3 days).

Figure 12. Wadati diagrams for four stations, using multiple events and assumed origin times.

Figure 13. Typical displacement spectra used in source studies. On left is P-wave recorded on FM tape system, center is P-wave recorded on digital system, and right is S-wave recorded digitally. FM signal is shown at higher gain than other two. Corner frequencies and data windows are indicated. Spectra of noise samples are shown dashed.

Figure 14. Moment - magnitude relations for Geysers microearthquakes (heavy lines), using the three different magnitudes, compared with other such relations (JM, Johnson and McEvilly, 1974; WB, Wyss and Brune, 1968; BL, Bakun and Lindh, 1977, TH, Thatcher and Hanks, 1973; BB, Bakun and Bufe, 1975). Dashed lines implies extrapolation from range of original data. M_{CL} and M_{CB} data from Tables 3 and 4a, M_L data from Table 4c.

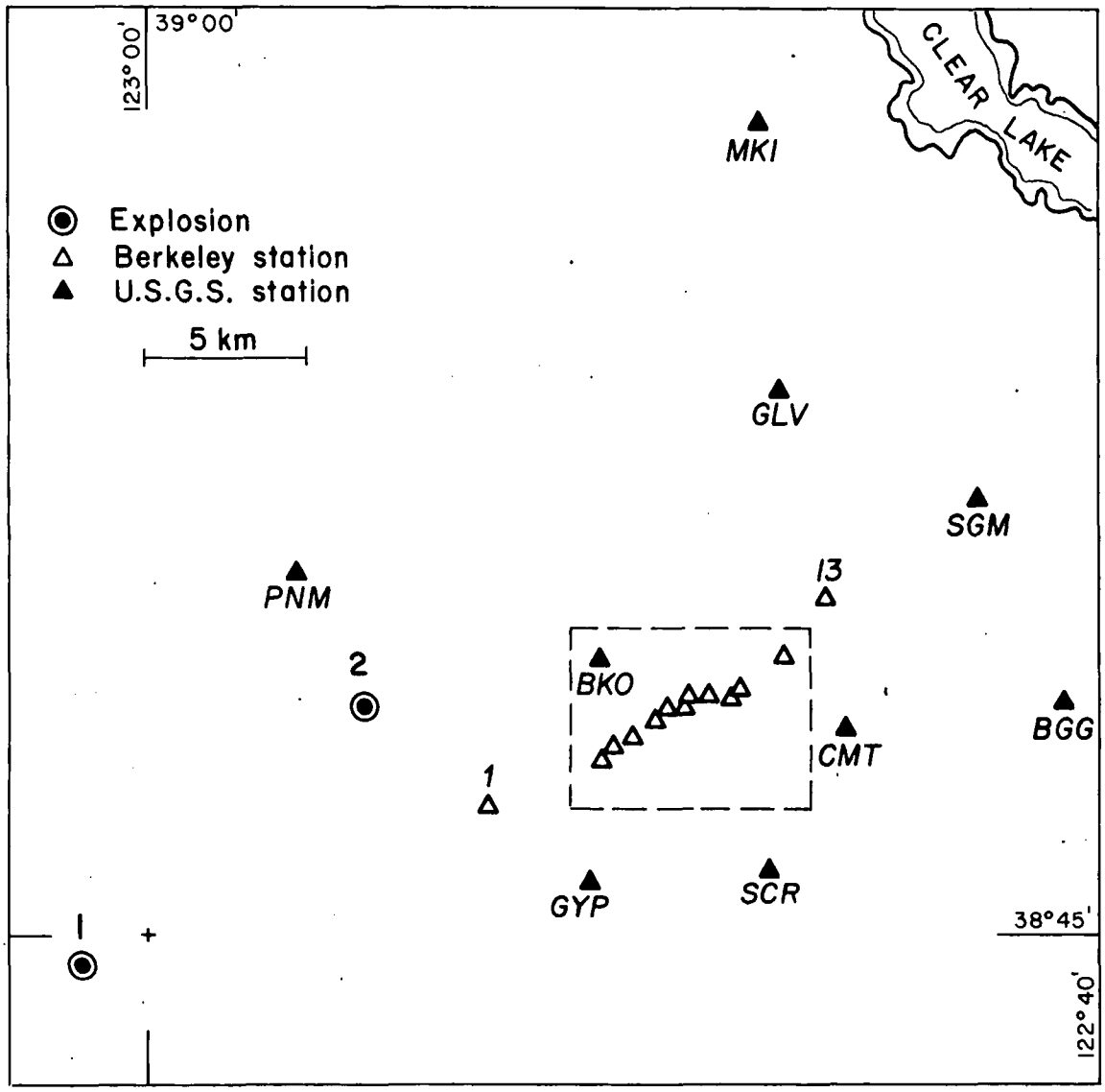

XBL 785-807

Fig. 1

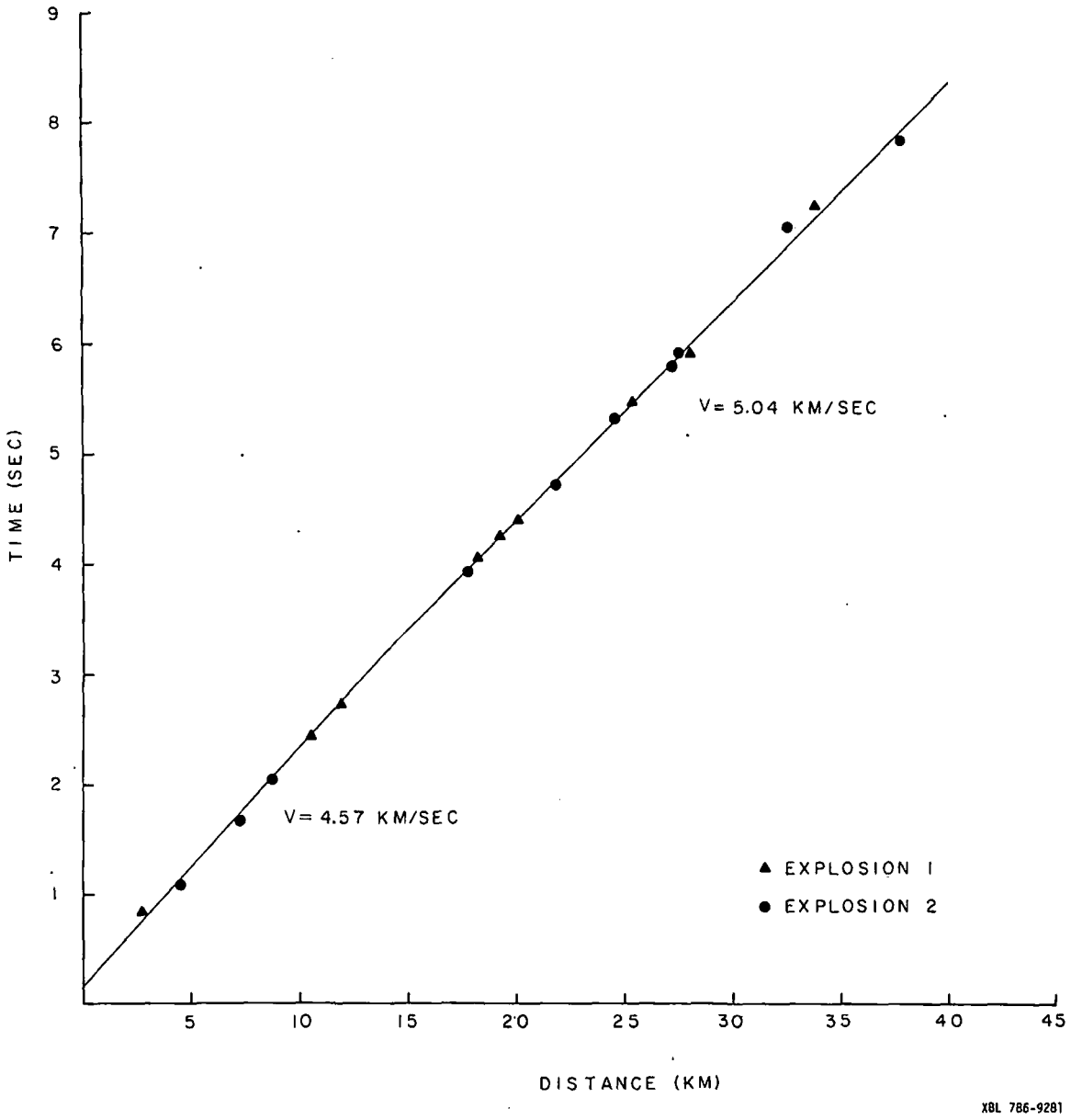
TIME (SEC)
DISTANCE (KM)
V= 4.57 KM/SEC
V= 5.04 KM/SEC
EXPLOSION 1
EXPLOSION 2
XBL 786-9281

Fig. 2

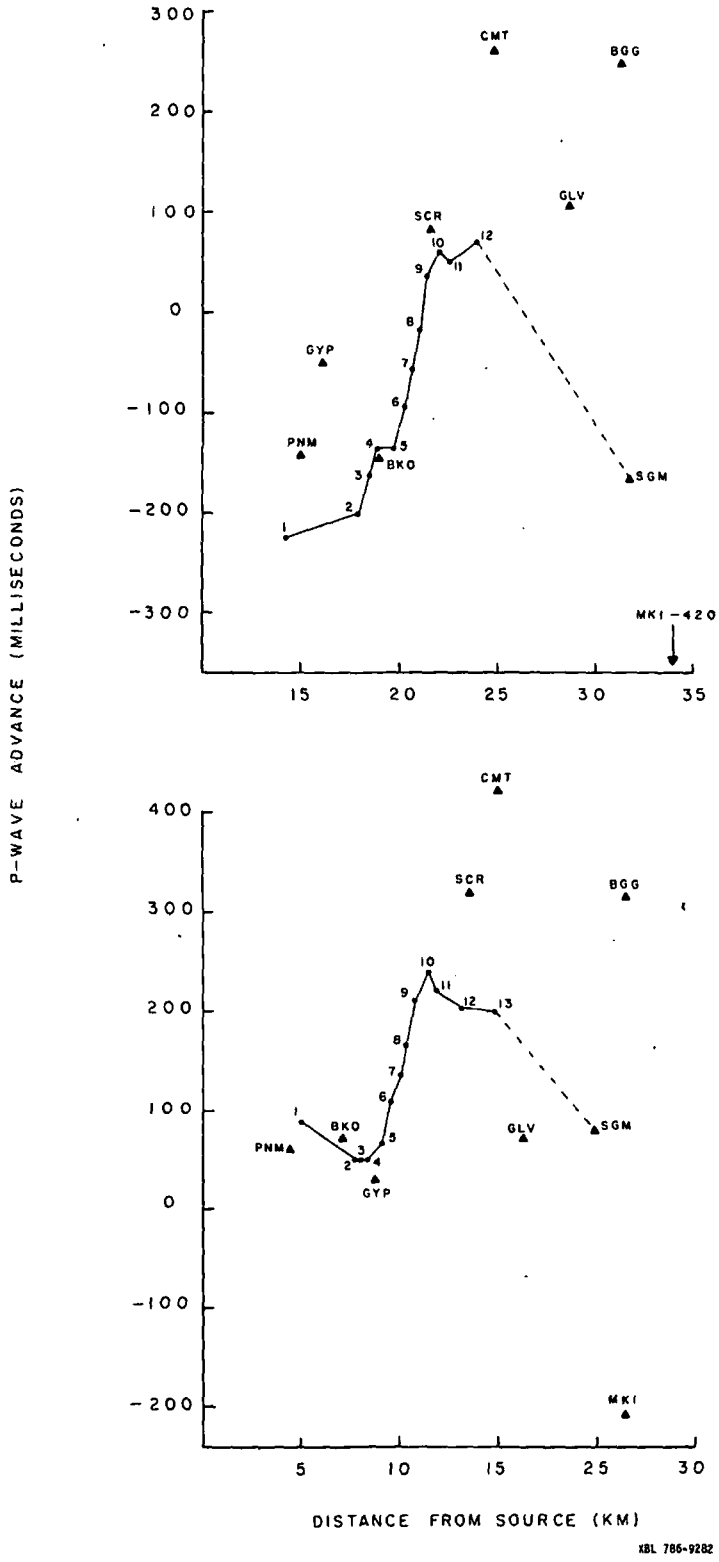
P-WAVE ADVANCE (MILLISECONDS)
300
200
100
0
-100
-200
-300
CMT
BGG
GLV
SCR
GYP
PNM
BKO
SGM
MKI -420
15
20
25
30
35
400
300
200
100
0
-100
-200
CMT
SCR
BGG
PNM
BKO
GYP
GLV
SGM
MKI
5
10
15
25
30
DISTANCE FROM SOURCE (KM)
XBL 786-9282

Fig. 3

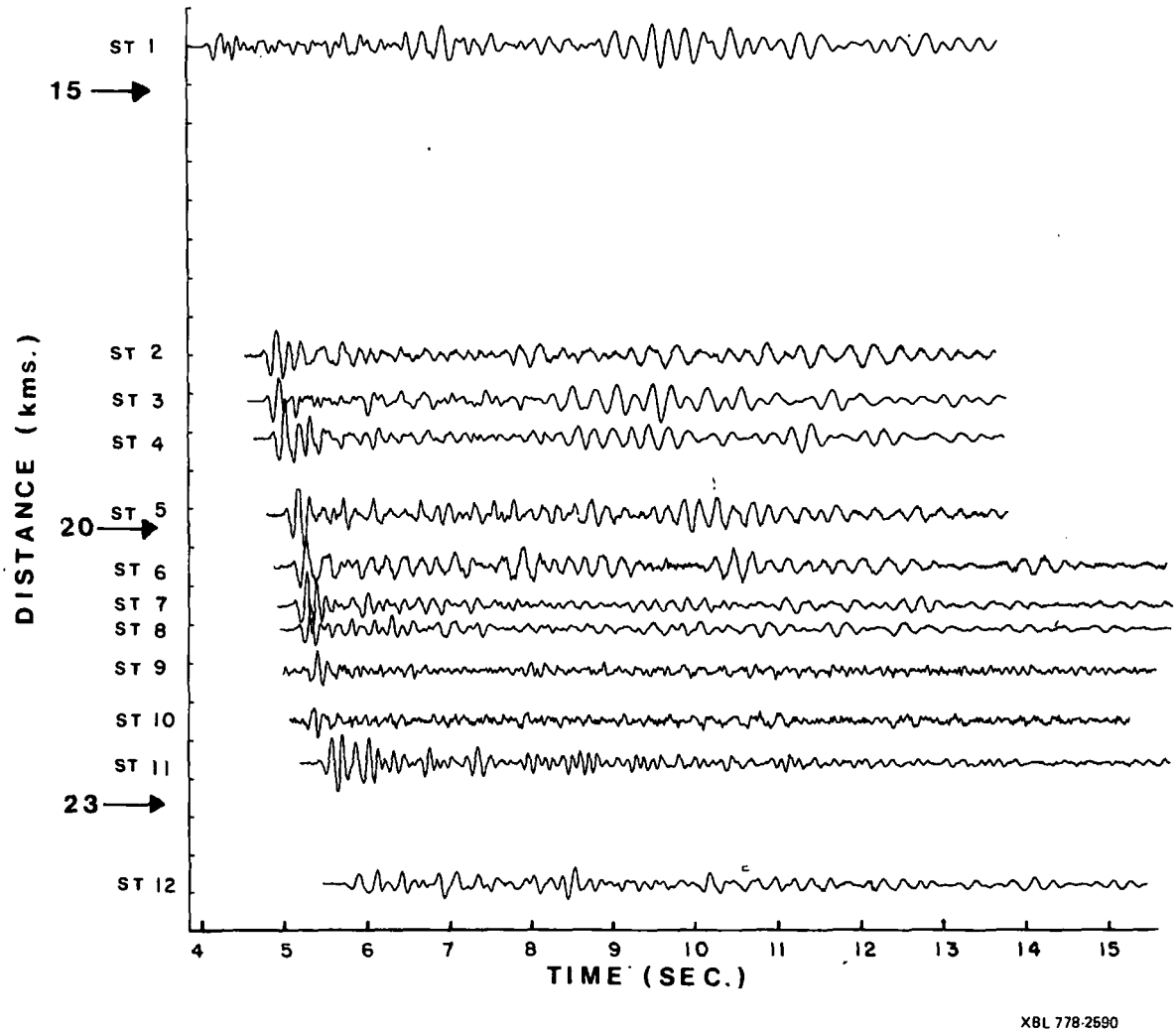
ST 1
15
ST 2
ST 3
ST 4
ST 5
20
ST 6
ST 7
ST 8
ST 9
ST 10
ST 11
23
ST 12
DISTANCE (kms.)
4
5
6
7
8
9
10
11
12
13
14
15
TIME (SEC.)
XBL 778-2590

Fig. 4

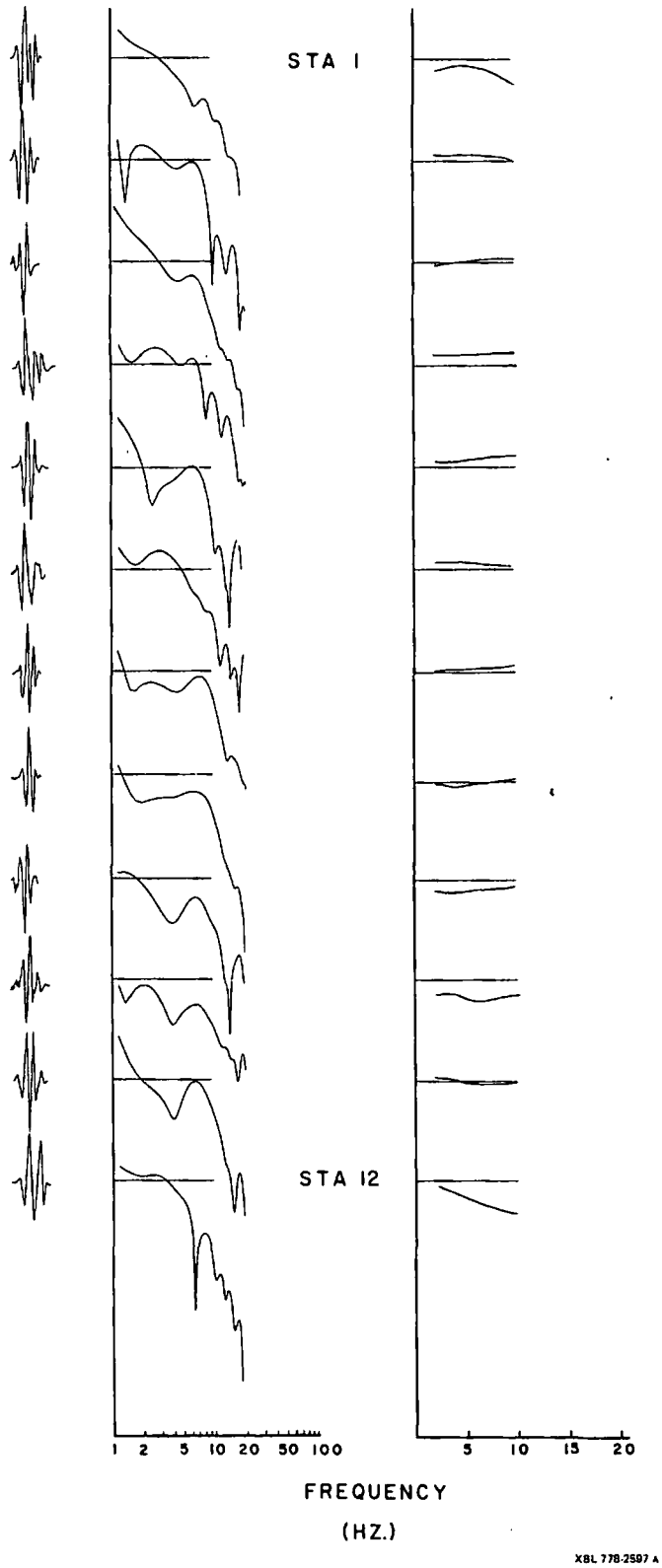
STA 1
STA 12
1 2 5 10 20 50 100
5 10 15 20
FREQUENCY
(HZ.)
XBL 778-2597 A

Fig. 5

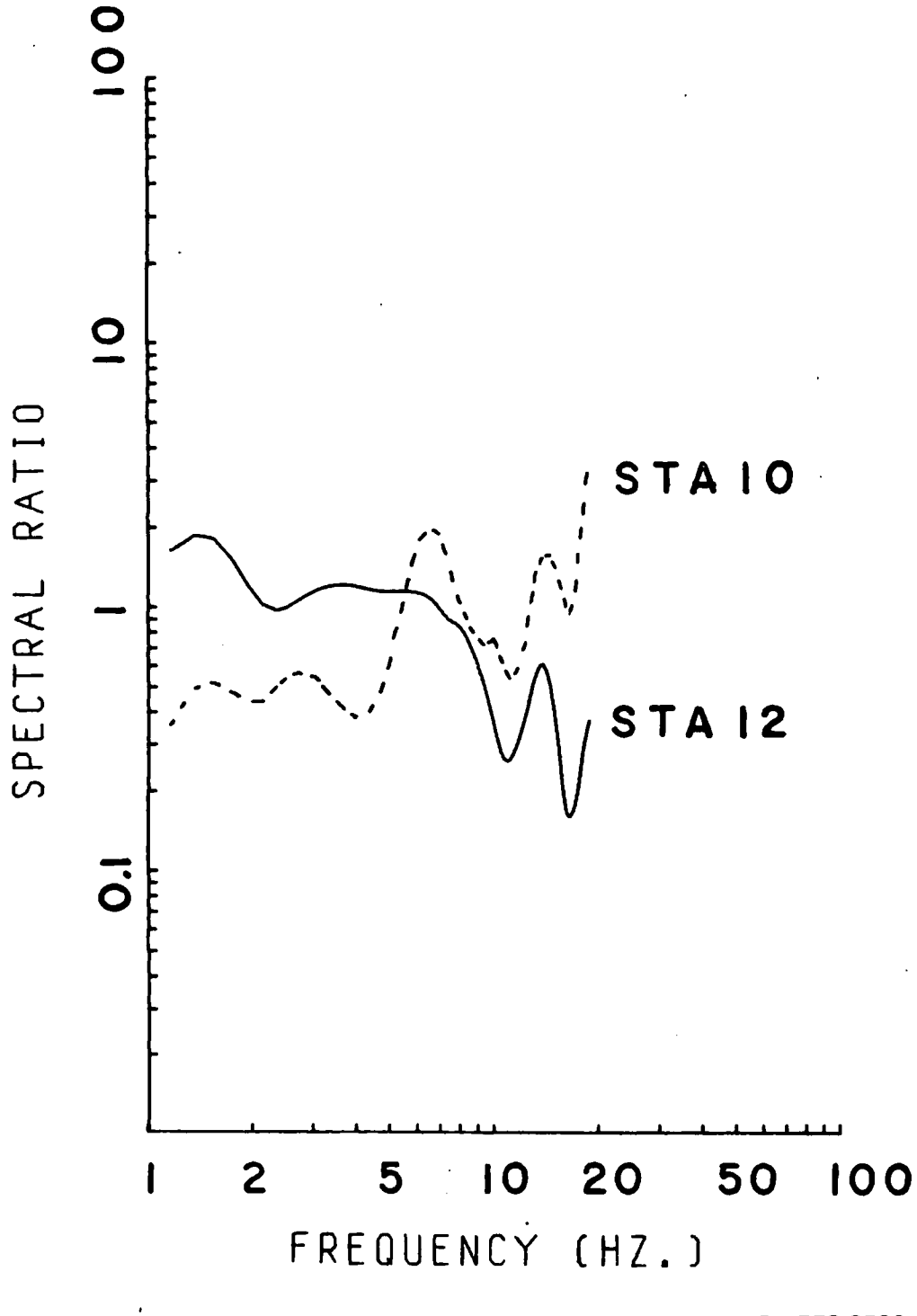
100
10
1
0.1
SPECTRAL RATIO
STA 10
STA 12
1
2
5
10
20
50
100
FREQUENCY (HZ.)
XBL 778-2589

Fig. 6

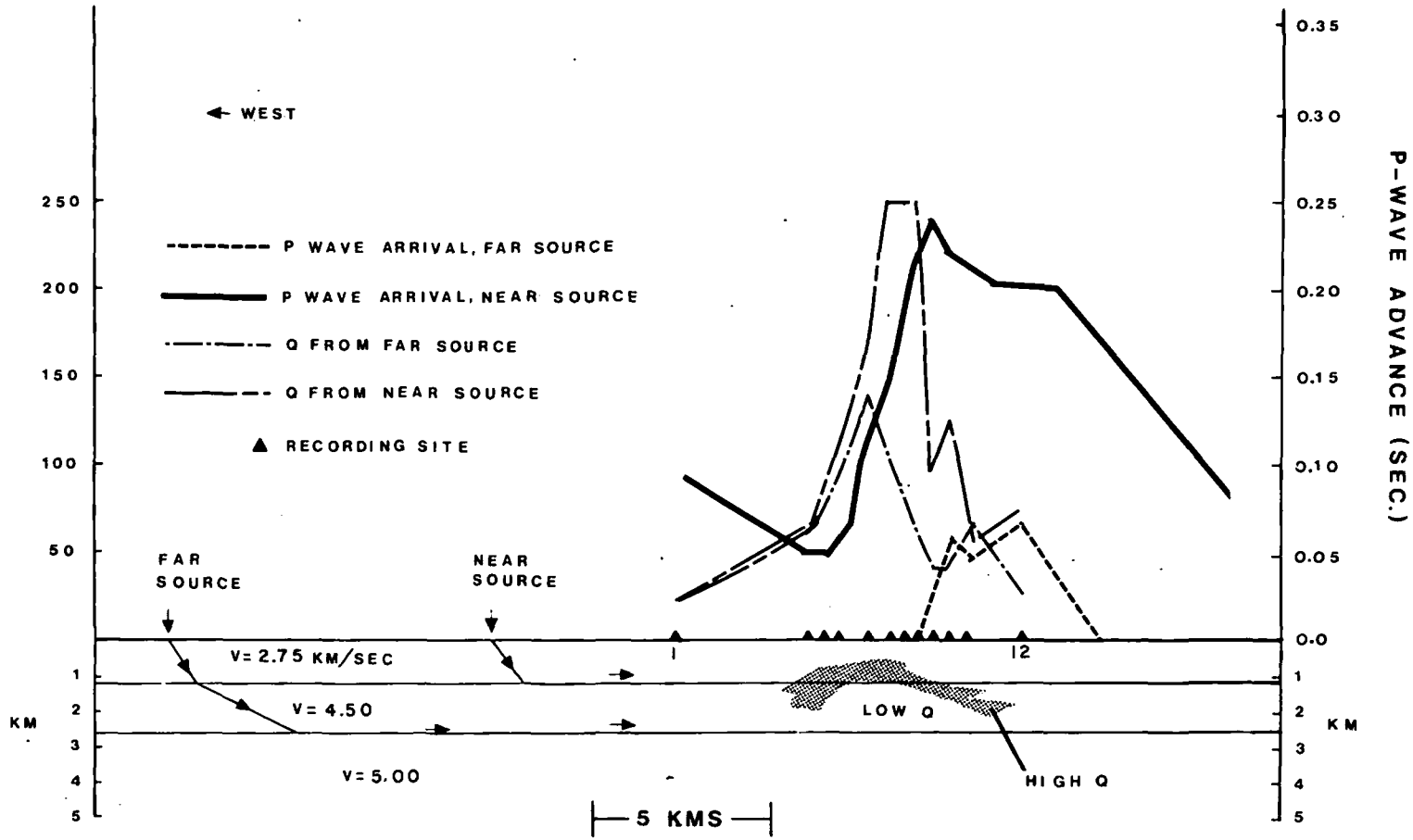

XBL 778-2593

Fig. 7

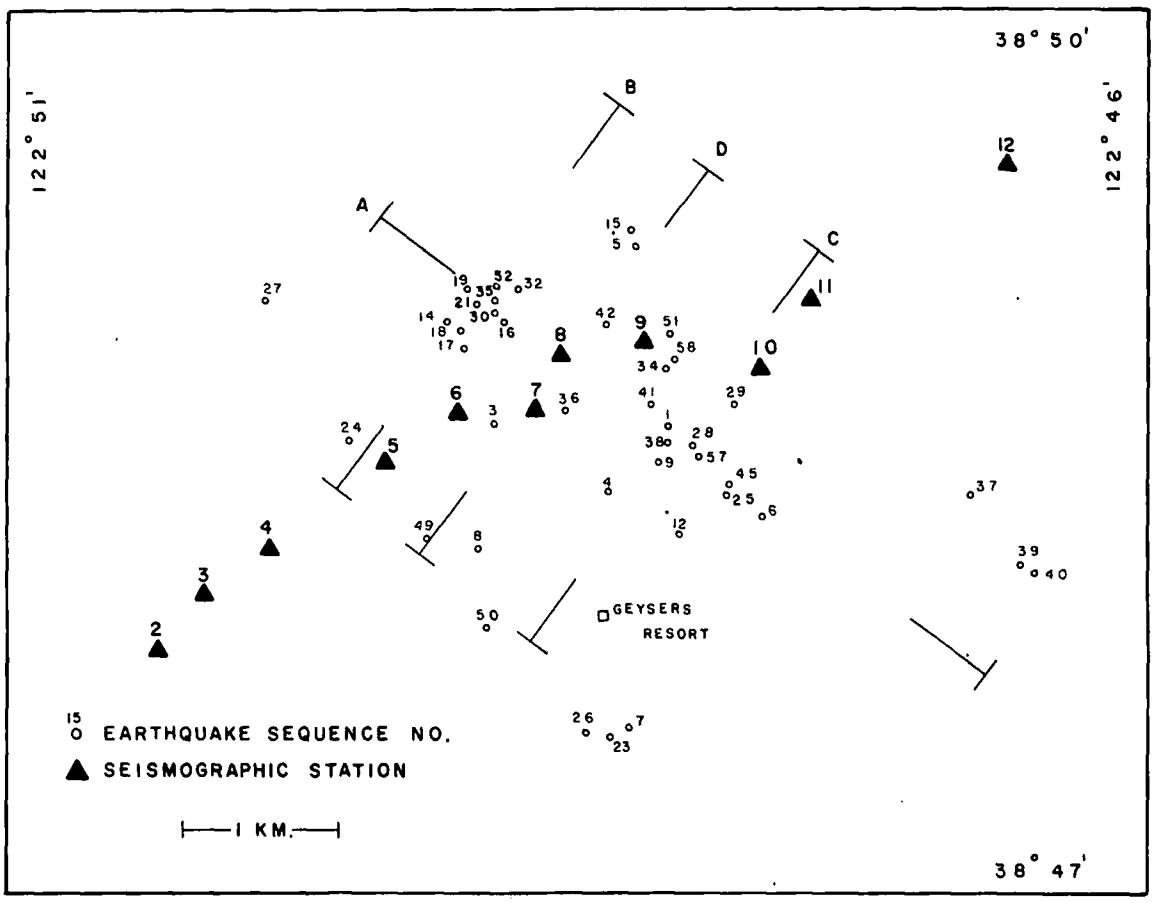

XBL 7612-10896

Fig. 8

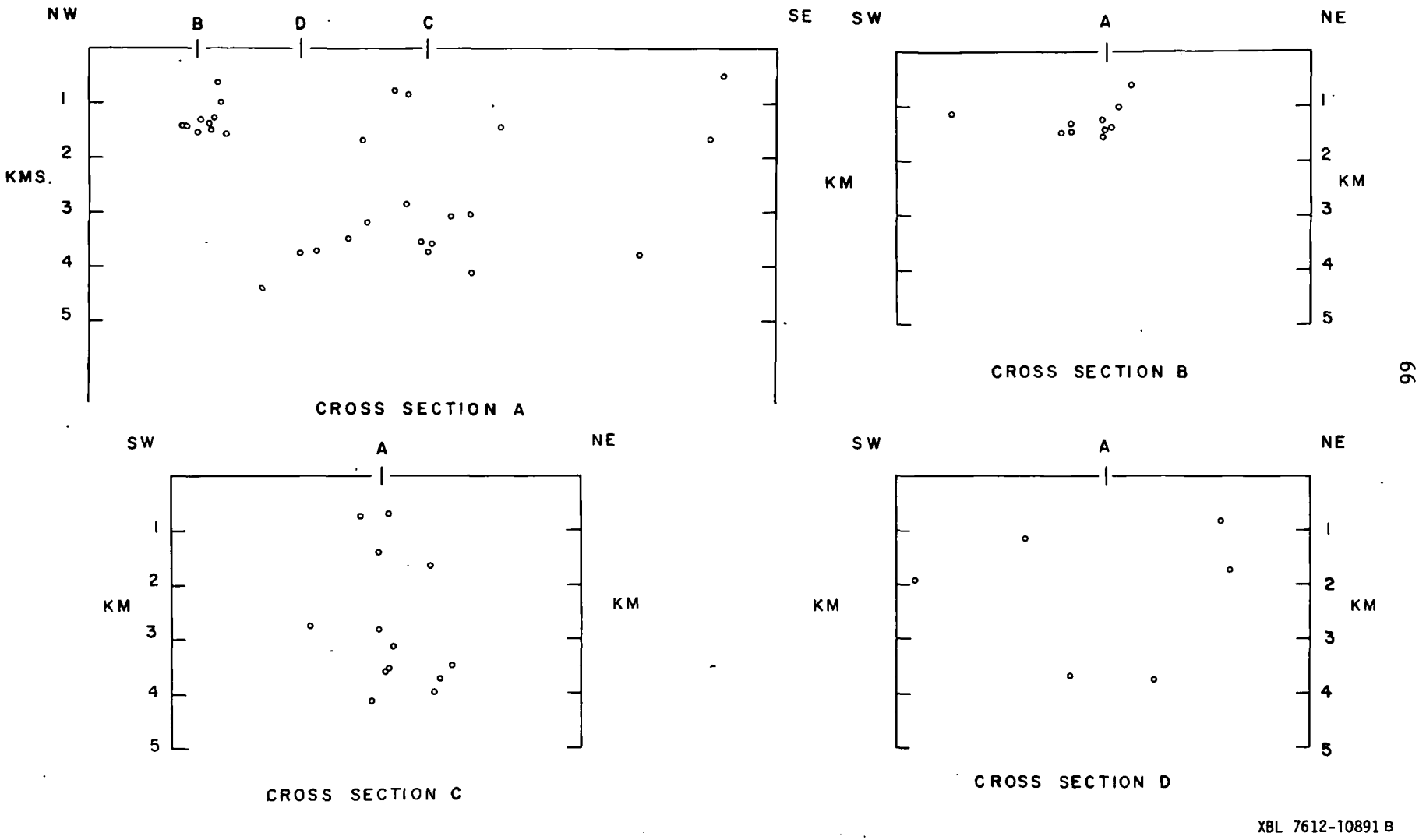
NW
B
D
C
SE
KMS.
1
2
3
4
5
CROSS SECTION A
SW
A
NE
KM
CROSS SECTION B
SW
A
NE
KM
KM
CROSS SECTION C
SW
A
NE
KM
KM
CROSS SECTION D
XBL 7612-10891 B

Fig. 9

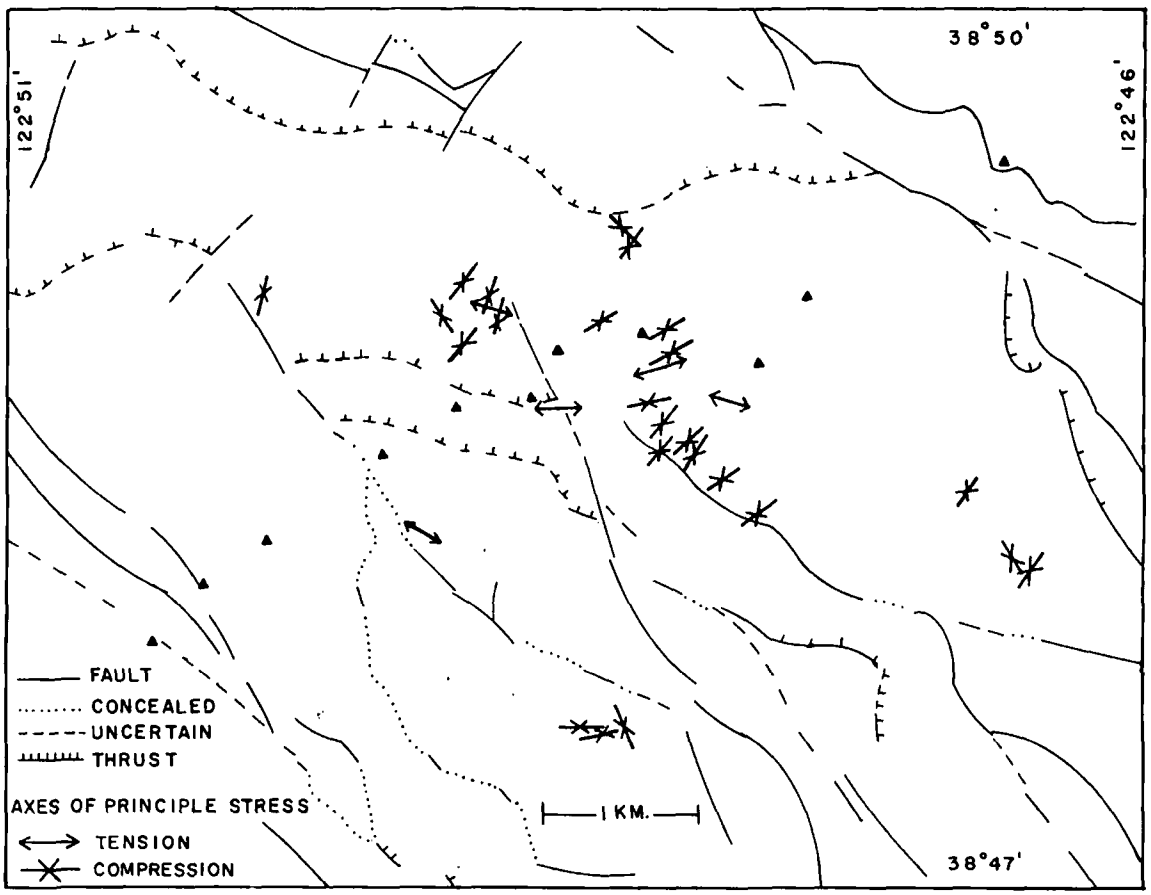

XBL 7612-10893

Fig. 10

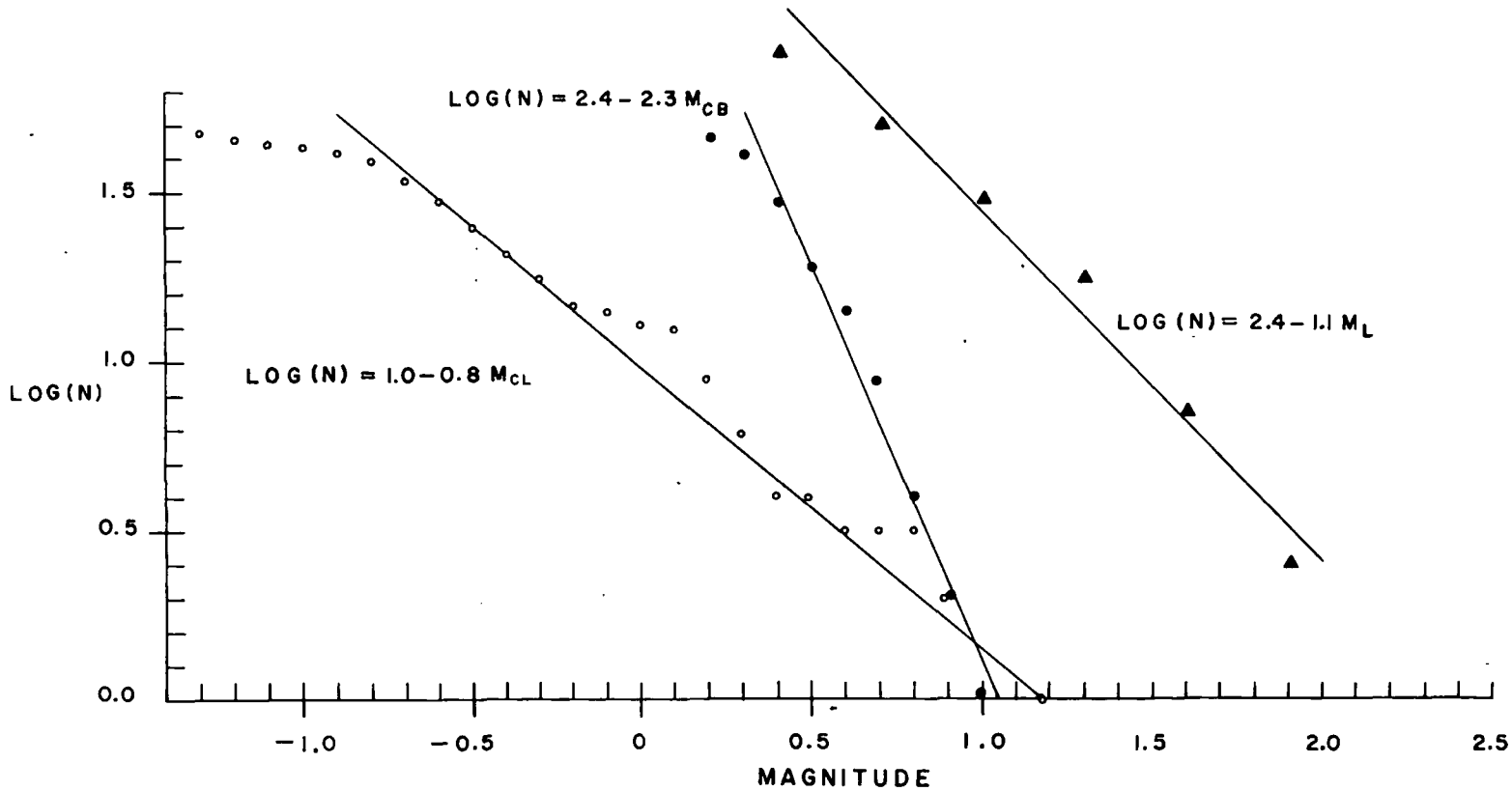

XBL 778-2591

Fig. 11

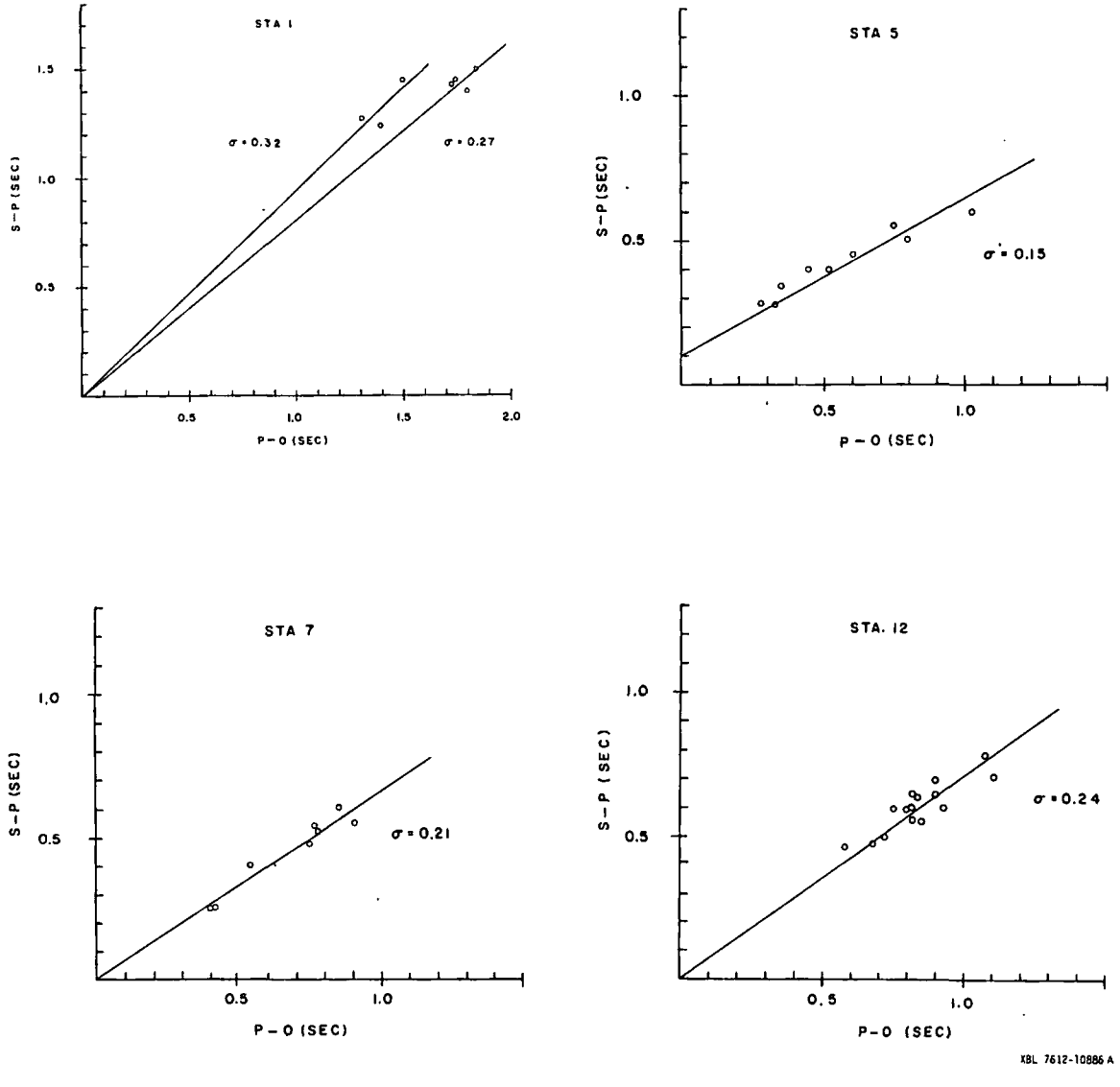
STA 1
σ = 0.32
σ = 0.27
S-P (SEC)
P-O (SEC)
STA 5
σ = 0.15
S-P (SEC)
P-O (SEC)
STA 7
σ = 0.21
S-P (SEC)
P-O (SEC)
STA. 12
σ = 0.24
S-P (SEC)
P-O (SEC)
XBL 7612-10886 A

Fig. 12

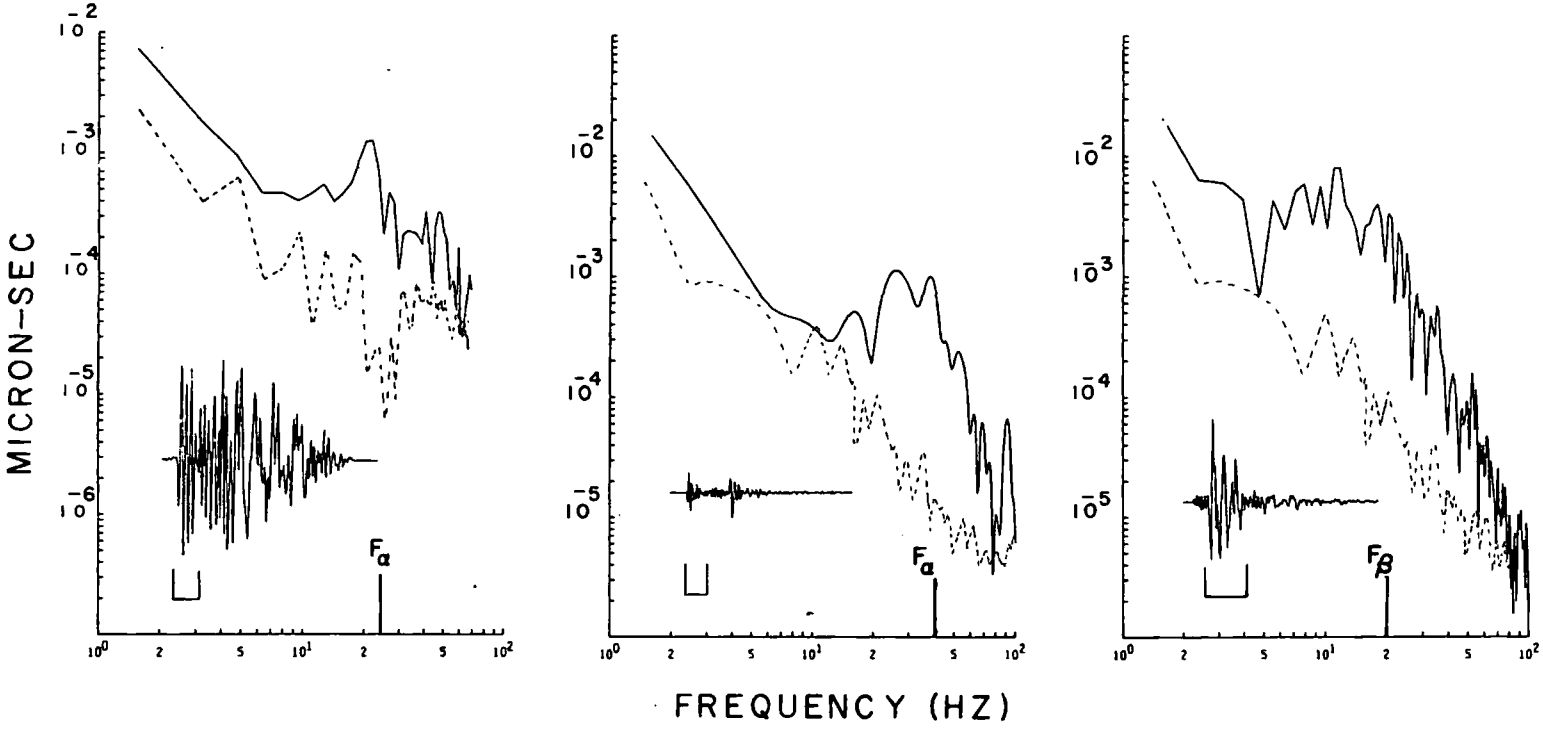

Fig. 13

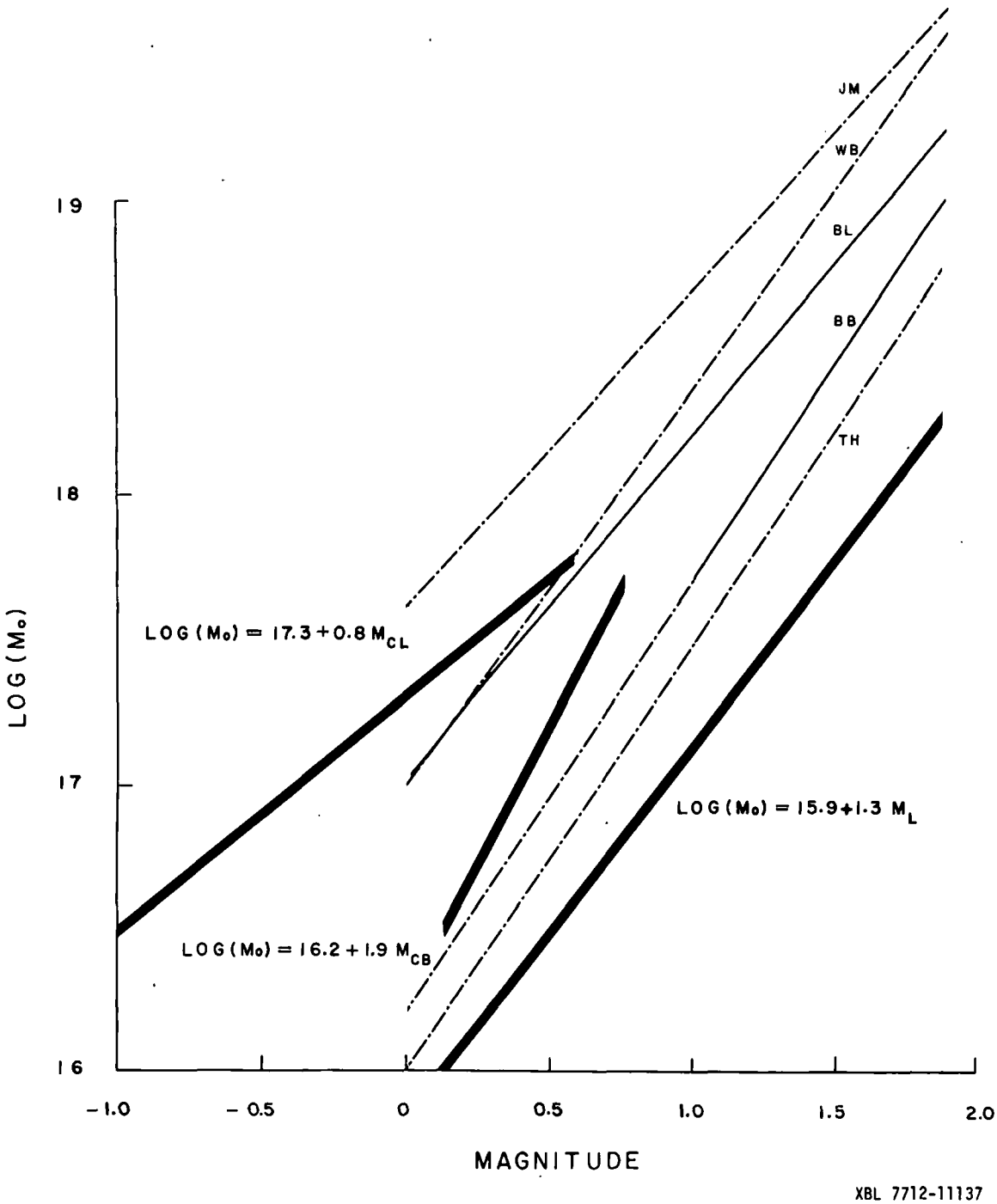
JM
WB
BL
BB
TH
19
18
17
16
LOG (M⊙)
LOG (M⊙) = 17.3 + 0.8 M_CL
LOG (M⊙) = 16.2 + 1.9 M_CB
LOG (M⊙) = 15.9 + 1.3 M_L
-1.0
-0.5
0
0.5
1.0
1.5
2.0
MAGNITUDE
XBL 7712-11137

Fig. 14

PHILLIP M. WRIGHT
UNIVERSITY OF UTAH RES. INST.
EARTH SCIENCE LABORATORY
RESEARCH PARK, 391 CHIPETA WAY
SALT LAKE CITY, UT 84102

986687